NEURODEGENERATIVE DISEASE

Cortical hyperexcitability in mouse models and patients with amyotrophic lateral sclerosis is linked to noradrenaline deficiency

Aurore Brunet[1]†, Cristina Benetton[2]†, Jelena Scekic-Zahirovic[1]†‡, XiaoQian Ye[3,4], Evgeny Logunov[3,4], Vincent Douchamps[5], Salim Megat[1], Virginie Andry[6], Vanessa Wing Yin Kan[3,4], Geoffrey Stuart-Lopez[1], Johan Gilet[1], Simon J. Guillot[1], Sylvie Dirrig-Grosch[1], Charlotte Gorin[1], Margaux Trombini[1], Stéphane Dieterle[1], Jérôme Sinniger[1], Mathieu Fischer[1], Frédérique René[1], Zeynep Gunes[3,4], Pascal Kessler[7], Luc Dupuis[1], Pierre-François Pradat[2,8], Yannick Goumon[6], Romain Goutagny[5], Véronique Marchand-Pauvert[2]*§, Sabine Liebscher[3,4,9,10]*§, Caroline Rouaux[1]*§

Amyotrophic lateral sclerosis (ALS) is a devastating neurodegenerative disease, characterized by the death of upper (UMN) and lower motor neurons (LMN) in the motor cortex, brainstem, and spinal cord. Despite decades of research, ALS remains incurable, challenging to diagnose, and of extremely rapid progression. A unifying feature of sporadic and familial forms of ALS is cortical hyperexcitability, which precedes symptom onset, negatively correlates with survival, and is sufficient to trigger neurodegeneration in rodents. Using electrocorticography in the *Sod1*^{G86R} and *Fus*$^{\Delta}$*NLS*/+ ALS mouse models and standard electroencephalography recordings in patients with sporadic ALS, we demonstrate a deficit in theta-gamma phase-amplitude coupling (PAC) in ALS. In mice, PAC deficits started before symptom onset, and in patients, PAC deficits correlated with the rate of disease progression. Using mass spectrometry analyses of CNS neuropeptides, we identified a presymptomatic reduction of noradrenaline (NA) in the motor cortex of ALS mouse models, further validated by in vivo two-photon imaging in behaving *SOD1*^{G93A} and *Fus*$^{\Delta}$*NLS*/+ mice, that revealed pronounced reduction of locomotion-associated NA release. NA deficits were also detected in postmortem tissues from patients with ALS, along with transcriptomic alterations of noradrenergic signaling pathways. Pharmacological ablation of noradrenergic neurons with DSP-4 reduced theta-gamma PAC in wild-type mice and administration of a synthetic precursor of NA augmented theta-gamma PAC in ALS mice. Our findings suggest theta-gamma PAC as means to assess and monitor cortical dysfunction in ALS and warrant further investigation of the NA system as a potential therapeutic target.

INTRODUCTION

The neurodegenerative disease amyotrophic lateral sclerosis (ALS) is primarily characterized by the death of upper (UMN) and lower motor neurons (LMN) in the motor cortex and bulbo-spinal segments, respectively (*1*). ALS is mostly a sporadic disease, but about 10% of the cases have a family history, two-thirds of which arise from mutations in *C9ORF72*, *SOD1*, *TARDBP*, and *FUS* genes (*2*). Because of the lack of effective treatments, the disease is fatal within only 2 to 5 years upon symptom onset (*2*). ALS diagnosis is often complicated because of clinical heterogeneity and the fact that UMN signs are more difficult to detect and can be masked by LMN signs (*1*), which greatly delays treatment initiation and limits inclusion in clinical trials. A large body of evidence, however, demonstrates early motor cortex impairment in ALS (*3*, *4*). A systematic investigation of cortical dysfunction thus bears the great potential for speeding up diagnosis and offering critical insight into pathogenesis.

Cortical impairment in ALS is associated with cortical hyperexcitability, which has been documented in sporadic and familial forms of ALS (*5*–*7*). It was shown to precede motor symptom onset in *SOD1* mutation carriers and sporadic ALS cases and to correlate with disease severity/progression (*5*). A corticofugal disease trajectory, in which the pathology is initiated in the cortex and spreads along anatomical projections to subcortical regions, was proposed (*3*). Recent studies in rodents further substantiate this notion. Chronic chemogenetic stimulation of parvalbumin (PV)–positive interneurons in the motor cortex of *SOD1*^{G93A} mice decreases UMN hyperexcitability and downstream LMN degeneration and increases mouse survival (*8*). Furthermore, cytoplasmically mislocalized TDP-43 in UMN of wild-type (WT) mice is sufficient to render them hyperexcitable and to induce the degeneration of downstream LMN (*9*).

Cortical hyperexcitability in patients with ALS has been thus far mainly assessed by using the gold standard paired-pulse transcranial magnetic stimulation (ppTMS) combined with electromyography

[1]Université de Strasbourg, Inserm UMRS 1329, Strasbourg Translational Neuroscience and Psychiatry (STEP), Centre de Recherche en Biomédecine de Strasbourg, 67000 Strasbourg, France. [2]Sorbonne Université, Inserm, CNRS, Laboratoire d'Imagerie Biomédicale, LIB, 75006 Paris, France. [3]Institute of Clinical Neuroimmunology, Klinikum der Universität München, Ludwig–Maximilians University Munich, 82152 Martinsried, Germany. [4]Biomedical Center, Ludwig–Maximilians University Munich, 82152 Martinsried, Germany. [5]Laboratoire de Neurosciences Cognitives et Adaptatives, CNRS UMR7364, Université de Strasbourg, 67000 Strasbourg, France. [6]CNRS UPR3212, SMPMS-INCI, Mass Spectrometry Facilities, Institut des Neurosciences Cellulaires et Intégratives, Centre National de la Recherche Scientifique and University of Strasbourg, 67 000 Strasbourg, France. [7]Inserm UMS 38, Centre de Recherche en Biomédecine de Strasbourg, Faculté de Médecine, Université de Strasbourg, 67000 Strasbourg, France. [8]Neurologie, AP-HP, Hôpital Pitié-Salpêtrière, 75013-Paris, France. [9]Munich Cluster for Systems Neurology (SyNergy), 81377 Munich, Germany. [10]Medical Faculty, University of Cologne and Department of Neurology, University Hospital of Cologne, Cologne, 50937 Germany.
*Corresponding author. Email: veronique.marchand-pauvert@inserm.fr (V.M.-P.); sabine.liebscher@med.uni-muenchen.de (S.L.); caroline.rouaux@inserm.fr (C.R.)
†These authors contributed equally to this work.
‡Present address: German Center for Neurodegenerative Diseases (DZNE), Ulm, Germany.
§These authors contributed equally to this work.

(*5*). However, the technique is often limited to the assessment of upper limb innervation, hinges critically on functional UMN-to-LMN and LMN-to-muscle connections, and can therefore not be implemented throughout disease progression as neurodegeneration advances. For the same reason, implementations in rodent models, which recapitulate UMN and LMN degeneration (*6, 7*), are hampered. Therefore, alternatives to ppTMS are needed to easily and reliably assess cortical dysfunction. Electroencephalography (EEG) in patients and electrocorticography (ECoG) in rodents offer these advantages through the investigation of brain oscillations and their interactions, without the need for LMN involvement. A phenomenon probed in cortical EEG is cross-frequency coupling and, in particular, phase-amplitude coupling (PAC), which refers to the modulation of the amplitude of a fast oscillation by the phase of a slow oscillation (*10*). Cross-frequency coupling in general and PAC in particular are seen as a means to coordinate neural activity across different spatial and temporal scales, through the interaction between large-scale brain networks that oscillate and synchronize at lower frequencies (delta, theta, alpha, and beta bands) and fast, local networks that are active at higher frequencies and required for effective computation and synaptic modification (gamma band) (*11*). In the neocortex, coupling has been reported between the amplitude of broadband gamma activity (>30 Hz) and the phase of low-frequency rhythms, including delta (0.5 to 4 Hz), theta (4 to 8 Hz), and alpha (8 to 13 Hz) (*11*). PAC is highly dependent on proper excitation/inhibition (E/I) balance (*11, 12*) and was shown to be compromised in neurodegenerative disorders, such as Parkinson's disease (PD) (*13, 14*) and Alzheimer's disease (AD) (*15*–*18*), and in frontotemporal dementia (FTD) (*19*). To our knowledge, PAC has not yet been investigated in ALS patients.

Despite evidence for its contribution to ALS pathophysiology in patients and rodent models (*5, 8, 9*), the cellular and molecular mechanisms underlying cortical hyperexcitability and LMN degeneration remain incompletely understood. Clinical ppTMS studies have revealed increased excitation and compromised inhibition, indicating circuit-level deficits (*5*). Preclinical studies have demonstrated early postnatal synaptic deficits in *SOD1*^{G93A} and *TDP-43*^{Q331K} transgenic mice, increased excitation onto UMNs, and increased excitability of cortical neurons in the *SOD1*^{G93A}, *TDP-43*^{A315T} (*6, 7*), and *Fus*$^{\Delta NLS/+}$ (*20*) mouse models of the disease. In addition, several lines of evidence indicate an involvement of cell types other than UMN, such as inhibitory interneurons (*8*) or glia cells (*21, 22*), arguing for more complex network changes. However, in addition to the main neurotransmitters, glutamate and γ-aminobutyric acid (GABA), other neurotransmitters and neuromodulators contribute to the fine tuning of motor cortex activity, which are less well studied (*6, 23*). These comprise, among others, serotonin, whose homeostasis is impaired in patients with ALS and mouse models of the disease (*24, 25*); dopamine, which is prominently altered in PD (*26*); and noradrenaline (NA), impaired in PD and AD (*27, 28*). Given the compelling evidence for an involvement of neuromodulators in the pathophysiology of other neurodegenerative diseases, we here hypothesized that they also play a role in ALS.

Using ECoG and EEG recordings in mice and humans, respectively, in vivo two-photon imaging in behaving mice, liquid chromatography–mass spectrometry (LC-MS), and histology and transcriptomics of human and mouse tissues, we here show that deficits in PAC are a traceable phenomenon in patients with ALS and mouse models, which was associated with cortical NA deficits. We also show that NA reduction can be successfully targeted pharmacologically, which acutely mitigates cortical hyperexcitability in mice.

RESULTS

Sod1^{G86R} and *Fus*$^{\Delta NLS/+}$ mice display increased susceptibility to pentylenetetrazol

We first wanted to investigate whether the cortical hyperexcitability described in patients with ALS translates into broader cortical network dysfunction and cortical hyperexcitability in ALS mouse models. To address these questions, we chose the BAC transgenic *Sod1*^{G86R} mouse model of ALS, maintained on the FVB/N background (*29*), and the knock-in *Fus*$^{\Delta NLS/+}$ mouse model of ALS and FTD, maintained on the C57Bl/6J background (*30*), for their genetic and phenotypic complementarity. Transgenic mice overexpressing a mutant murine *Sod1*^{G86R} gene present with initial loss of UMN by 60 days, muscle denervation, and progressive motor impairments by 90 days, followed by ultimate LMN degeneration and death of the animals by 105 to 120 days of age (Fig. 1A) (*29, 31*). Knock-in *Fus*$^{\Delta NLS/+}$ mice instead express a truncated form of *Fus* in one of the two endogenous alleles and display spontaneous hyperactivity by 4 months and mild motor impairments along with cognitive and behavioral deficits by 10 months of age (Fig. 1B) (*20, 30*). We first submitted *Sod1*^{G86R} and *Fus*$^{\Delta NLS/+}$ to the pentylenetetrazol (PTZ) susceptibility test, using ECoG (Fig. 1, A to C). PTZ is a noncompetitive γ-aminobutyric acid type A ($GABA_A$) receptor antagonist used to unravel network hyperexcitability in animal models of epilepsy and neurodegeneration (*32, 33*). We administered a single subconvulsive dose of PTZ (30 mg/kg) to 85-day-old *Sod1*^{G86R} and 4-month-old *Fus*$^{\Delta NLS/+}$ animals and respective WT littermates. All injected animals arrested their behavior without any overt tonic-clonic seizures. We then computed the number of epileptiform-like events in ECoG traces before and after PTZ injection (Fig. 1, D to I). In *Sod1*^{G86R} animals, we found significantly increased number of events ($P < 0.0001$, Fig. 1F) and decreased latency to the first event ($P = 0.0043$, Fig. 1G) compared with their WT littermates. We observed the same results in *Fus*$^{\Delta NLS/+}$ mice, with significantly increased number of events ($P = 0.03025$, Fig. 1H) and decreased latency ($P = 0.0037$, Fig. 1I) compared with WT littermates. Mice on the FVB/N background displayed a greater response to PTZ than mice on the C57Bl/6J background, in accordance with former reports (*34, 35*). These results indicate that *Sod1*^{G86R} and *Fus*$^{\Delta NLS/+}$ mouse models of ALS display cortical network hyperexcitability, revealed by increased susceptibility to PTZ.

Sod1^{G86R} and *Fus*$^{\Delta NLS/+}$ mice display impaired theta-gamma PAC

To longitudinally assess cortical network dysfunction in mouse models of ALS, we further used ECoG recordings to conduct PAC analyses (Fig. 2A). Theta-gamma PAC is highly dependent on proper E/I balance (*11, 12*), with gamma frequency synchrony attributed to interconnected fast-spiking $GABA_A$-expressing interneurons (*11*) and theta frequency attributed to cortical excitatory neurons and more particularly to layer V pyramidal neurons of the human brain (*36, 37*). In addition, rodent and human motor cortices were reported to exhibit strong theta-gamma coupling (*38*–*40*). To assess PAC, we chose the method of the modulation index (MI) developed by Tort *et al.* (*41, 42*) for its noise tolerance and amplitude independence. We ran longitudinal ECoG recordings from

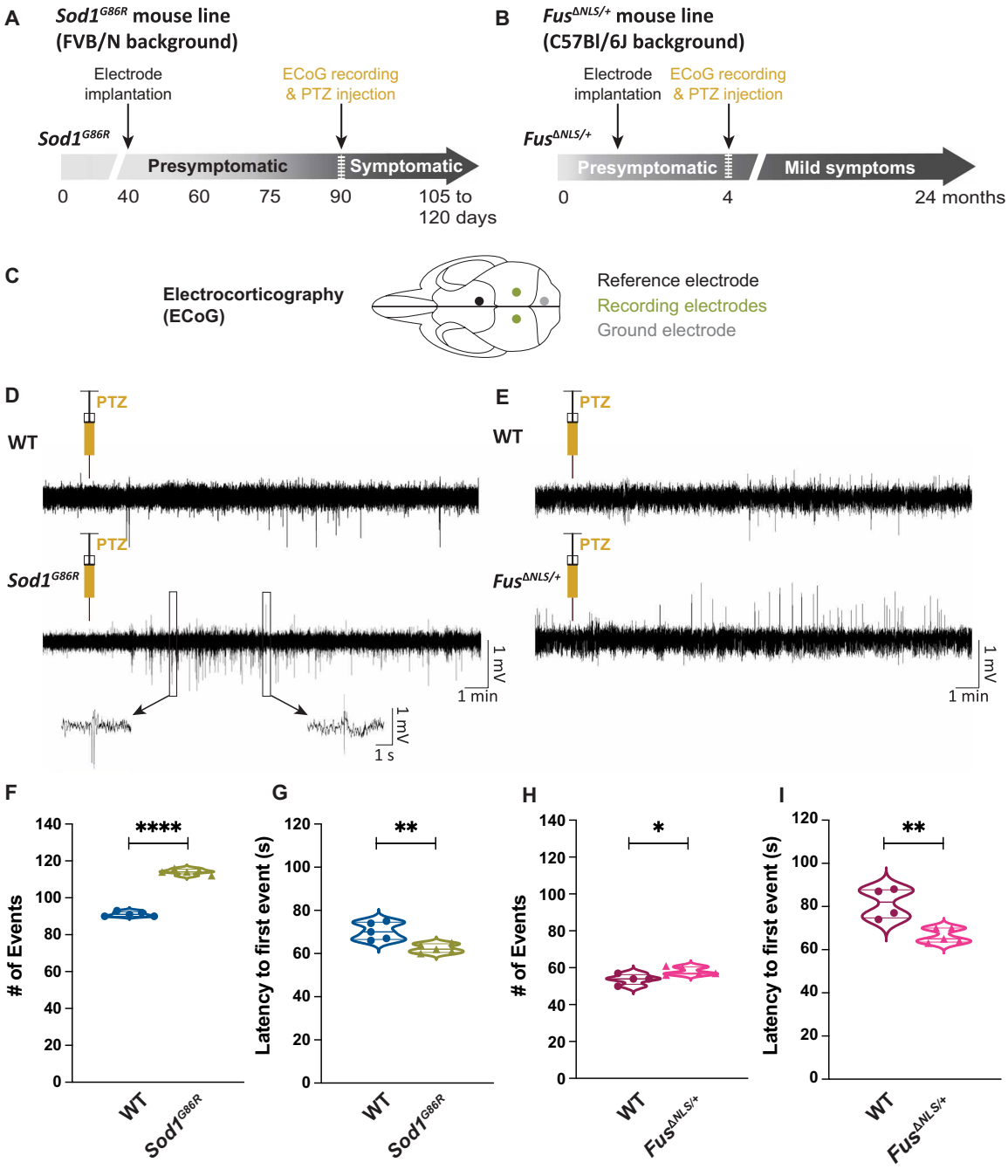

Fig. 1. *Sod1*^{G86R} and *Fus*$^{\Delta NLS/+}$ mice exhibit cortical hyperexcitability. (**A** and **B**) Genetic background and time course of disease onset and progression in the *Sod1*^{G86R} and *Fus*$^{\Delta NLS/+}$ mouse models of ALS. (**C**) Schematic representation of the positioning of subdural electrodes used for ECoG. (**D** and **E**) Representative ECoG traces before (10 min in total, only 2 min are represented) and after (20 min) a single injection of PTZ (30 mg/kg) of *Sod1*^{G86R} (D) and *Fus*$^{\Delta NLS/+}$ (E) mice and control littermates. (**F**) Quantification of the number of epileptiform-like events displayed by *Sod1*^{G86R} and controls during the first 10 min that immediately followed PTZ administration. (**G**) Latency to first epileptiform-like event upon PTZ injection of *Sod1*^{G86R} mice and their WT littermates. (**H**) Quantification of the number of epileptiform-like events displayed by *Fus*$^{\Delta NLS/+}$ mice and controls during the first 10 min that immediately followed PTZ administration. (**I**) Latency to first epileptiform-like event upon PTZ injection of *Fus*$^{\Delta NLS/+}$ mice and their WT littermates. $n = 5$ WT and 5 *Sod1*^{G86R} female mice; $n = 4$ WT females and 4 *Fus*$^{\Delta NLS/+}$ female mice. Two-sided unpaired Student's t test; $^{*}P < 0.05$; $^{**}P < 0.01$; $^{****}P < 0.0001$.

subdural electrodes positioned over the sensorimotor areas (Fig. 1C) and performed PAC analyses in rapid eye movement (REM) sleep (Fig. 2) and active wakefulness (Fig. 3), two states known to display theta-gamma PAC in rodents (*43*), from the presymptomatic stage (45 days) until disease end-stage (105 days) in *Sod1*^{G86R} mice and from presymptomatic (3 months) to symptomatic (11 months) stages in *Fus*$^{\Delta NLS/+}$ mice. As expected during REM sleep, comodulograms displayed coupling between theta and low gamma (T-LG;

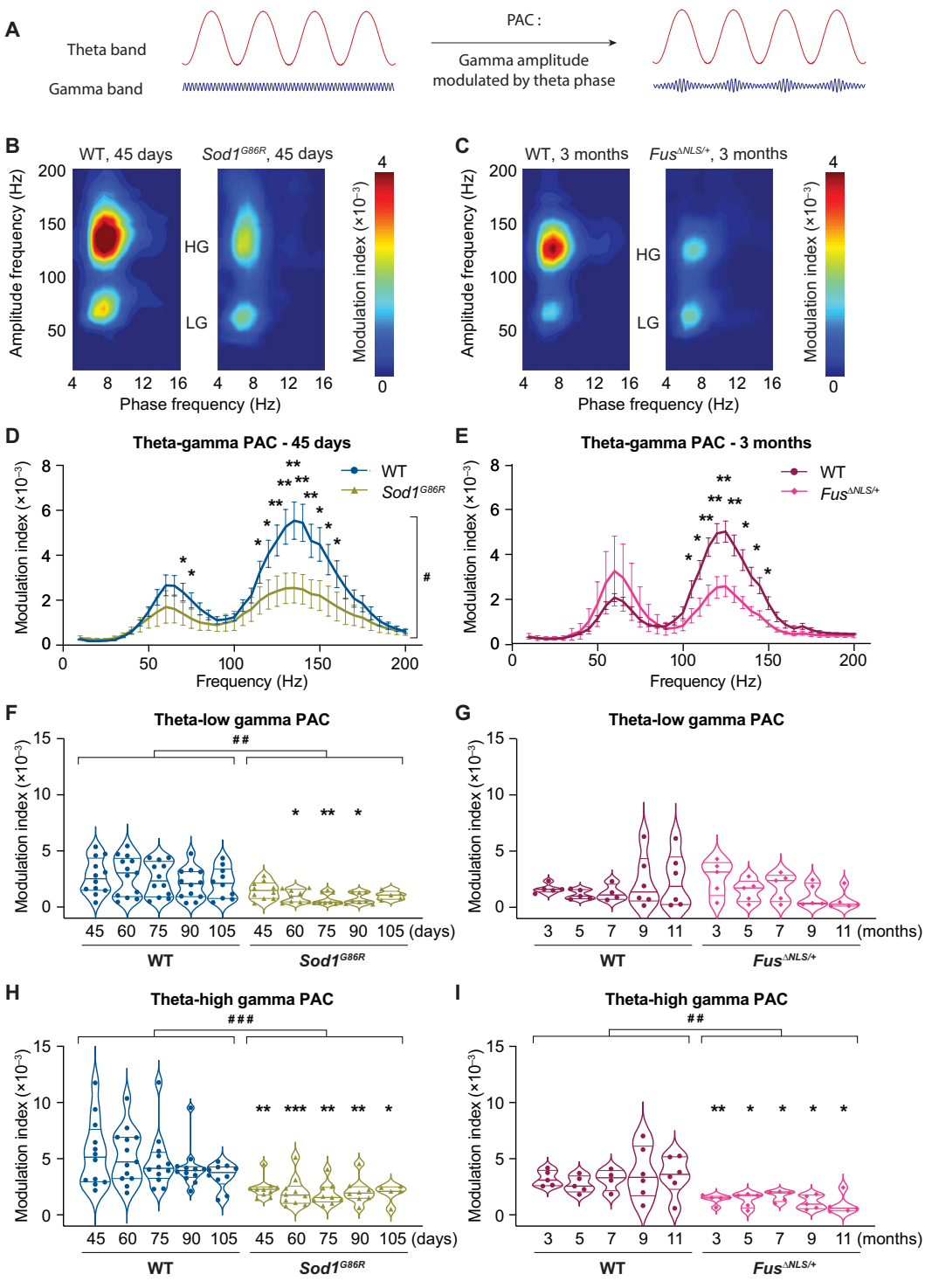

Fig. 2. *Sod1*^{G86R} and *Fus*$^{\Delta NLS/+}$ mice display presymptomatic and sustained decreased T-HG PAC during REM sleep. (**A**) Schematic representation of theta (red) and gamma (blue) waves and theta-gamma PAC (right). (**B** and **C**) Representative comodulation phase-amplitude maps from 45-day-old WT and *Sod1*^{G86R} mice (B) and 3-month-old WT and *Fus*$^{\Delta NLS/+}$ mice (C) during REM sleep. Color gradients represent the MI. HG, high gamma; LG, low gamma. (**D** and **E**) Graphs representing the MI across frequencies in 45-day-old WT and *Sod1*^{G86R} mice (D) and 3-month-old WT and *Fus*$^{\Delta NLS/+}$ mice (E) during REM sleep. (**F** and **G**) Graphs representing the longitudinal T-LG PAC of WT and *Sod1*^{G86R} mice (F) and WT and *Fus*$^{\Delta NLS/+}$ mice (G) during REM sleep. (**H** and **I**) Graphs representing the longitudinal T-HG PAC of WT and *Sod1*^{G86R} mice (H) and WT and *Fus*$^{\Delta NLS/+}$ mice (I) during REM sleep. $n = 13$ WT and 10 *Sod1*^{G86R} male mice; $n = 6$ WT and 5 *Fus*$^{\Delta NLS/+}$ male mice. Two-way ANOVA (D and E) or mixed-effect analysis (F to I) followed by multiple comparisons test. #$P < 0.05$; ##$P < 0.01$; ####$P < 0.0001$ for genotype effect in two-way ANOVA or mixed-effect analysis and *$P < 0.05$; **$P < 0.01$; ***$P < 0.001$ in pairwise comparisons with age-matched WT controls.

around 60 Hz) and theta and high gamma (T-HG; around 120 Hz) (Fig. 2, B and C). At the earliest recorded ages, *Sod1*^{G86R} and *Fus*$^{\Delta NLS/+}$ animals demonstrated impaired theta gamma PAC during REM sleep (Fig. 2, D and E). T-LG PAC was differentially affected in the two mouse lines. Whereas the MI was significantly decreased in the *Sod1*^{G86R} (Fig. 2F; genotype effect: $P = 0.0073$ in mixed-effect analysis), it was not altered in the *Fus*$^{\Delta NLS/+}$ animals (Fig. 2G). T-HG PAC instead was significantly decreased in both mouse lines (Fig. 2, H and I; genotype effect: $P = 0.0007$ for *Sod1*^{G86R} and 0.0039 for *Fus*$^{\Delta NLS/+}$ in mixed-effect analysis), from the first recordings, and remained as such throughout the disease course. Power spectrum analysis revealed that LG and HG powers were unaffected in both lines (fig. S1, A to D). Theta power was significantly decreased in *Sod1*^{G86R} animals (fig. S1E; genotype effect: $P = 0.0009$ in mixed-effect analysis) but remained unchanged in *Fus*$^{\Delta NLS/+}$ mice (fig. S1F). Similarly, total power was significantly decreased in *Sod1*^{G86R} animals (fig. S1G; genotype effect: $P = 0.0028$ in mixed-effect analysis) and unchanged in *Fus*$^{\Delta NLS/+}$ mice (fig. S1H), ruling out the possibility that the decreased T-HG PAC revealed in both mouse lines during REM sleep was solely due to a power effect. We further analyzed theta-gamma PAC during active wakefulness (Fig. 3). As expected for this state of vigilance *(43)*, comodulograms displayed only T-LG PAC (Fig. 3, A and B), with lower MIs compared with REM sleep. At the first recorded ages, we found a decrease of the MI corresponding to LG frequencies in *Sod1*^{G86R} animals (Fig. 3C) but not in the *Fus*$^{\Delta NLS/+}$ mice (Fig. 3D). Decreased MI was maintained throughout the whole disease duration in *Sod1*^{G86R} mice (Fig. 3E; genotype effect: $P = 0.0004$ in mixed-effect analysis) but remained unchanged in the *Fus*$^{\Delta NLS/+}$ animals compared to controls (Fig. 3F). Decreased T-LG PAC in the *Sod1*^{G86R} line was accompanied by decreased total and theta powers (fig. S2, A and B; genotype effect: $P = 0.0022$ and 0.0012, respectively, in mixed-effect analysis), but LG and HG powers remained unaffected (fig. S2, C and D). In *Fus*$^{\Delta NLS/+}$ mice, powers remained unchanged

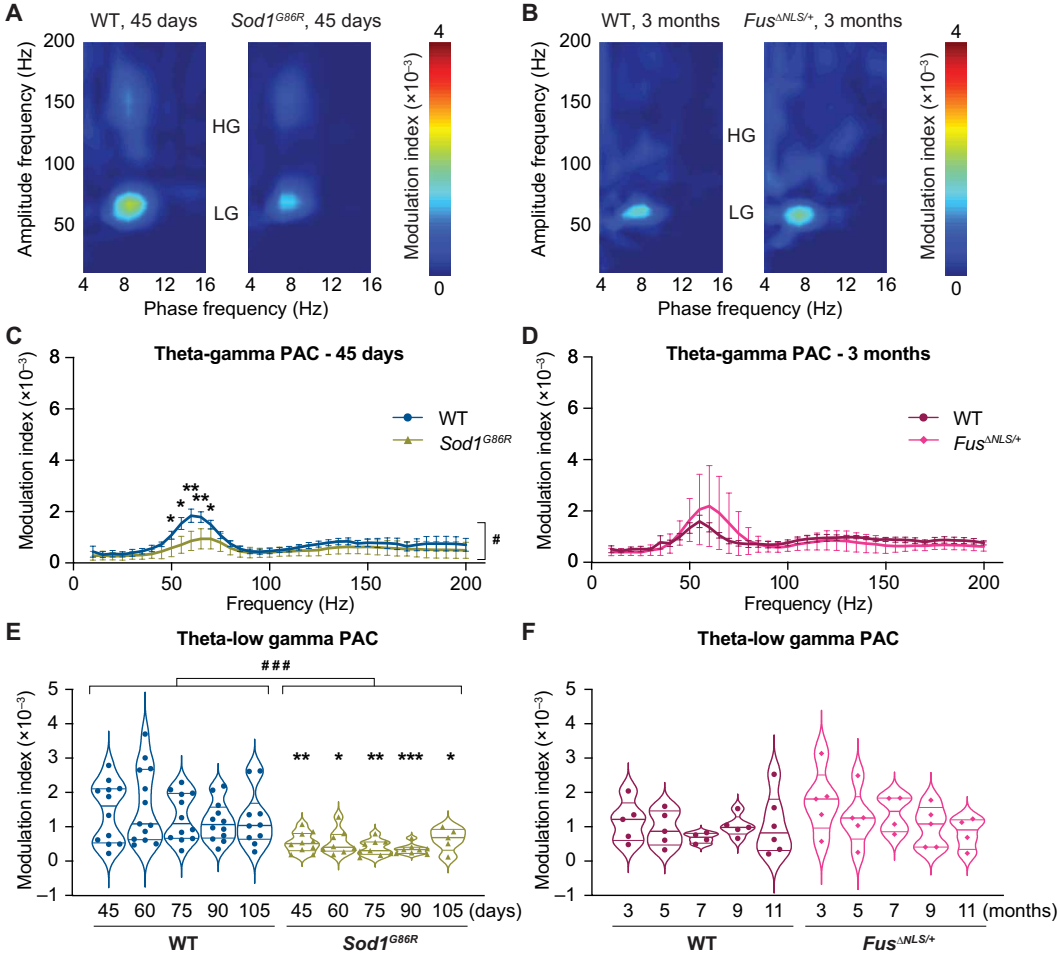

Fig. 3. *Sod1*^{G86R} mice display presymptomatic and sustained alteration of T-LG PAC during active wake. (**A** and **B**) Representative comodulation phase-amplitude maps from 45-day-old WT and *Sod1*^{G86R} mice (A) and 3-month-old WT and *Fus*$^{\Delta NLS/+}$ mice (B) during active wake. Color gradients represent the MI. HG, high gamma; LG, low gamma. (**C** and **D**) Graphs representing the MI across frequencies in 45-day-old WT and *Sod1*^{G86R} mice (C) and 3-month-old WT and *Fus*$^{\Delta NLS/+}$ mice (D) during active wake. (**E** and **F**) Graphs representing the longitudinal T-LG PAC of WT and *Sod1*^{G86R} mice from presymptomatic ages (45 and 60 days) to disease end stage (105 days) (E) and WT and *Fus*$^{\Delta NLS/+}$ mice from the presymptomatic age of 3 months until the symptomatic age of 11 months (F) during active wake. $n = 13$ WT and 10 *Sod1*^{G86R} male mice; $n = 6$ WT and 5 *Fus*$^{\Delta NLS/+}$ male mice. Two-way ANOVA (C and D) or mixed-effect analysis (E and F) followed by multiple comparisons test. ###$P < 0.001$ for genotype effect in two-way ANOVA of mixed-effect analysis and *$P < 0.05$; **$P < 0.01$; ***$P < 0.001$ in pairwise comparisons with age-matched WT controls.

except for LG power that was decreased (fig. S2, E to H; genotype effect: $P = 0.0112$ in mixed-effect analysis). Together, the data reveal that *Sod1*^{G86R} and *Fus*$^{\Delta NLS/+}$ animals present with common altered cortical network function that translates into decreased T-HG PAC during REM sleep. In addition, the *Sod1*^{G86R} mouse model of ALS also presents with decreased T-LG PAC during both REM sleep and active wakefulness, prompting us to test whether such a phenotype could be observed in patients with ALS during wakefulness.

Patients with sporadic ALS display impaired theta-gamma PAC in resting state

We performed resting state EEG (rsEEG) recordings and theta-gamma PAC analyses (Fig. 4A) on 26 patients with sporadic ALS (Table 1) and an age- and sex-matched group of 26 healthy individuals, focusing on the motor cortex (*38*–*40*). Electrodes were located above the sensorimotor areas (C_3 and C_4) and the interhemispheric sulcus (F_z, C_z, and P_z) that can also capture EEG signals from neighboring motor cortex, and recording was performed on every participant successively with eyes open (EO) and eyes closed (EC). We generated comodulograms for each of the five electrodes of both patients and controls, in both the EO and EC conditions (Fig. 4B), and extracted the mean MI for each condition (Fig. 4C). To evaluate the influence of (i) the recording condition (EO versus EC), (ii) the recording site (channels), and (iii) the group affiliation (controls versus ALS), we built a repeated-measures linear mixed-effect model (rmLMM). The analysis revealed that theta-gamma PAC was significantly stronger in the EO compared with the EC condition ($P < 0.0001$; Fig. 4C and fig. S3A), that the recording site presented a significant influence ($P < 0.0001$; fig. S3B), and that theta-gamma PAC was significantly lower in patients with ALS compared with controls ($P = 0.0043$; Fig. 4C and fig. S3C). Post hoc analysis further revealed a significant decrease of theta-gamma PAC in patients with ALS both in the EO and EC conditions ($P = 0.0133$ and 0.0194, respectively; Fig. 4C), driven by a selective effect at the level of C_3 ($P = 0.0061$ and $P < 0.0001$ in the EO and EC conditions, respectively; Fig. 4C). The signal power in the theta and gamma bands, as well as the absolute power, was not statistically different between controls and patients with ALS (fig. S3, D to F), ruling out the possibility that decreased theta-gamma PAC arose from altered powers. We further focused our analysis on the C_3 channel in the EC condition that showed the stronger effect (reduced by 63.83% in ALS patients compared to controls, $P < 0.0001$) and tested whether EC C_3 theta-gamma PAC correlated with the main clinical features of patients with ALS. We found no correlation between the patient's mean MI and site of onset ($P = 0.9572$; fig. S4A), UMN score ($P = 0.8033$; fig. S4B), revised amyotrophic lateral sclerosis functional rating scale (ALSFRS-r, $P = 0.0535$; fig. S4C), or disease duration ($P = 0.3822$; fig. S4D). However, patients' EC C_3 theta-gamma PAC significantly correlated with the disease progression rate ($P = 0.0323$; Fig. 4D). No correlation was found between the absolute power measured of C_3 in the EC condition and the main clinical features (fig. S4, E to I). Last, stratification of patients into slow and fast progressors (Table 1) confirmed that fast progressors displayed a significantly lower EC C_3 theta-gamma PAC than the slow progressors ($P = 0.0265$; Fig. 4E). Together, the data indicate that theta-gamma PAC recorded in EC conditions over the left sensorimotor area (C_3) is significantly decreased in patients with sporadic ALS compared with healthy controls and correlates with the progressive deterioration of motor functions.

Sod1^{G86R} and *Fus*$^{\Delta NLS/+}$ mice display altered cortical noradrenergic signaling

To test whether altered neurotransmitter signaling could explain cortical hyperexcitability in *Sod1*^{G86R} and *Fus*$^{\Delta NLS/+}$ mice, we conducted LC-MS analyses on microdissected motor cortex samples from 45-, 60-, and 90-day-old *Sod1*^{G86R} and 4-month-old *Fus*$^{\Delta NLS/+}$ mice and their age-matched control littermates to measure the concentration of the two main cortical neurotransmitters (glutamate and GABA) and relevant neuromodulators (glycine, serotonin, dopamine, and NA) (*23*). In *Sod1*^{G86R} mice compared with controls, glutamate was decreased [genotype effect: $P = 0.0189$ in two-way analysis of variance (ANOVA); fig. S5A]. GABA was unchanged (fig. S5B), but glycine was decreased (genotype effect: $P = 0.0040$ respectively in two-way ANOVA; fig. S5C). Whereas dopamine was unchanged (fig. S5D), serotonin was significantly decreased in *Sod1*^{G86R} animals (genotype effect: $P = 0.0034$ in two-way ANOVA; fig. S5E), as already reported (*24, 25*). None of these neurotransmitters and neuromodulators were affected in the *Fus*$^{\Delta NLS/+}$ mice compared to their WT littermates (fig. S5, F to J). NA was significantly decreased by 35.24 ± 2.81% in *Sod1*^{G86R} mice (genotype effect, $P < 0.0001$ in two-way ANOVA; Fig. 5A) and by 19.06 ± 2.65% in *Fus*$^{\Delta NLS/+}$ mice ($P = 0.0019$ in two-tailed Student's t test; Fig. 5A). Similar results were observed in the hippocampus and spinal cord of *Sod1*^{G86R} mice (genotype effect: $P < 0.0001$ in two-way ANOVA for both structures; fig. S6, A and B) but not in the spinal cord of *Fus*$^{\Delta NLS/+}$ animals (fig. S6C), pointing to differences in the extent of noradrenergic depletion across regions of the central nervous system and mouse lines. We observed that animals from the *Fus*$^{\Delta NLS/+}$ mouse line (WT and mutant) displayed, on average, four times higher NA tissue concentration than animals from the *Sod1*^{G86R} mouse line (WT and mutant), which is likely due to their respective genetic backgrounds (Fig. 1, A and B), as already reported (*44*).

To further investigate the origins of decreased cortical NA in *Sod1*^{G86R} and *Fus*$^{\Delta NLS/+}$ mice, we labeled and quantified the number of tyrosine hydroxylase (TH)–positive NA neurons in the locus coeruleus (LC), which harbors noradrenergic projection neurons innervating the cerebral cortex and spinal cord (fig. S7), and the density of dopamine-beta-hydroxylase (DBH)–positive noradrenergic projections to the motor cortex (Fig. 5, B and C). We found an overall significant decrease of TH-positive neurons of 20.93 ± 3.04% on average in the LC of *Sod1*^{G86R} mice compared with their WT littermates (mixed-effect analysis, genotype effect: $P = 0.0026$; fig. S7, A and B). However, paired post hoc comparisons revealed a significant decrease of TH-positive neurons in the LC of *Sod1*^{G86R} mice only at 45 days ($P = 0.0005$ at 45 days, $P = 0.2114$ at 60 days, and $P = 0.0795$ at 90 days). In addition, we did not detect any change in soma size (fig. S7C) of TH-positive neurons in the LC of *Sod1*^{G86R} animals. No difference in the number or size of TH-positive neurons was found in the *Fus*$^{\Delta NLS/+}$ animals (fig. S7, A to C). However, both mouse lines displayed a significantly decreased density of cortical DBH-positive fibers compared with controls (14.4 ± 2.66%, genotype effect: $P < 0.0001$ in mixed-effect analysis for *Sod1*^{G86R} mice; 7.40 ± 1.15%, $P = 0.0289$ in two-tailed Student's t test for *Fus*$^{\Delta NLS/+}$ mice; Fig. 5C), arguing for a more pronounced effect of the *Sod1*^{G86R} and *Fus*$^{\Delta NLS/+}$mutations on noradrenergic axons than on noradrenergic cell bodies. Next, we injected a retrograde adenovirus encoding *GFP* under the human *SYNAPSIN* promoter into the motor cortex of 85-day-old old *Sod1*^{G86R} and WT littermates (fig. S7D) and quantified the number of GFP-positive neurons

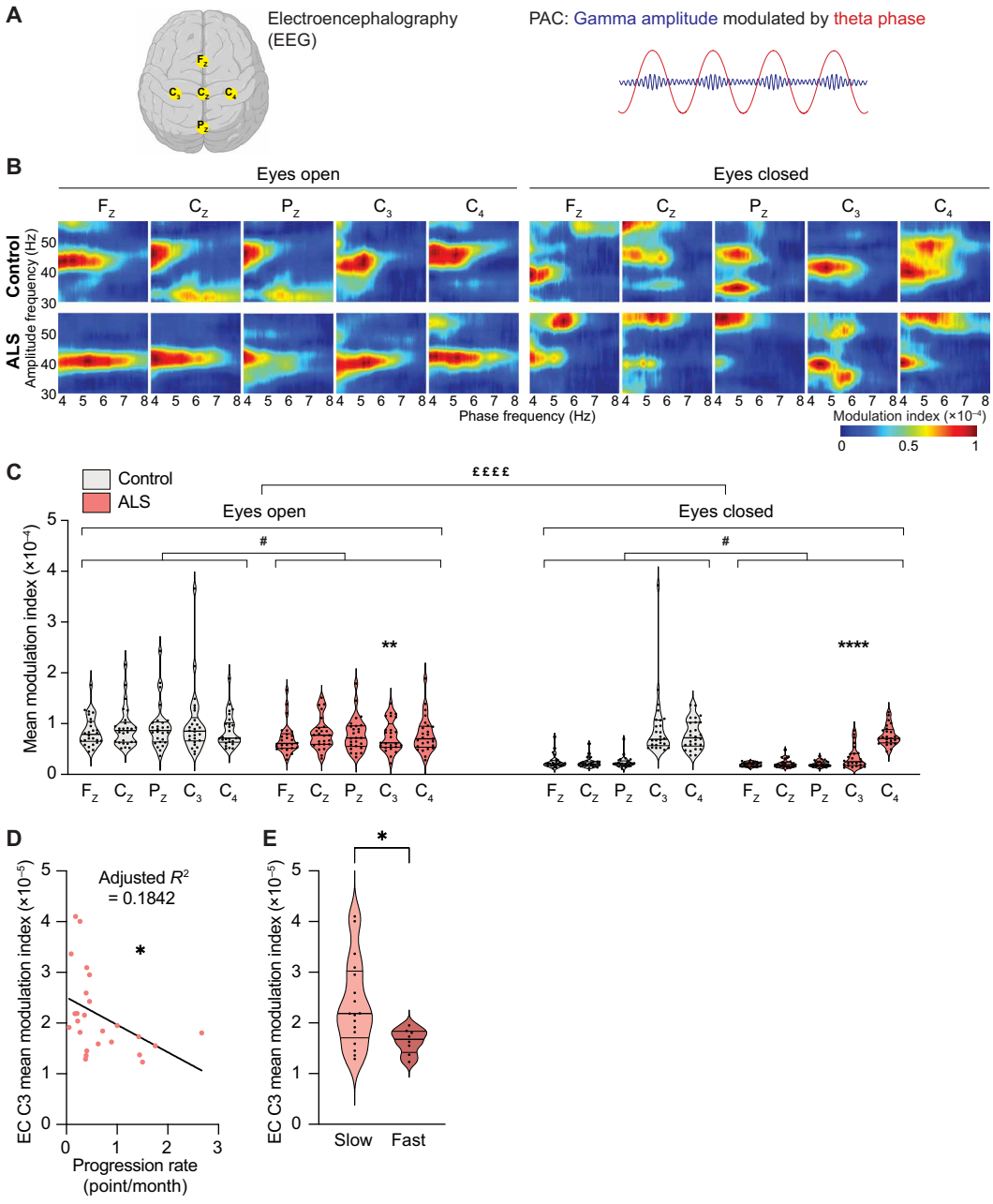

Fig. 4. Patients with sporadic ALS display decreased theta-gamma PAC over the left sensory motor cortex during EC rsEEG. (**A**) Schematic representation of the positioning of the electrodes of interest, over the sensorimotor areas (C_3 and C_4) and along the interhemispheric sulcus: (F_z, C_z, and P_z) (left) and schematic representation of theta-gamma PAC (right). (**B**) Representative comodulation phase-amplitude maps from one healthy participant (control) and one patient (ALS). Color gradients represent the MI. (**C**) Graphs representing the mean MI of healthy individuals (gray) and patients with sporadic ALS (coral) in rsEEG. (**D**) Correlation between C_3 mean MI of patients with ALS and their disease progression rate. (**E**) Graph representing the C_3 mean MI of patients with ALS subdivided between fast versus slow progressors. $n = 26$ controls and 26 patients with ALS. Repeated-measures linear mixed-effect model (rmLMM) followed by multiple comparisons test with $^{££££}P < 0.0001$ comparing EO and EC conditions; #$P < 0.05$ between patients and controls in either EO or EC condition and **$P < 0.01$ and ****$P < 0.001$ in pairwise comparisons between healthy controls and patients with ALS for a given condition (EO or closed) and electrode (C). Multiple regression analysis with *$P < 0.05$ (D). Two-tailed unpaired t test with *$P < 0.05$ (E).

present in the LC of the animals 5 days later (fig. S7, E to G). WT and *Sod1*^{G86R} mice displayed comparable amounts of TH- and GFP-positive noradrenergic neurons (fig. S7, F and G). Together, the data suggest that, in the *Sod1*^{G86R} and *Fus*$^{\Delta NLS/+}$ mouse lines, noradrenergic neurons projecting to the motor cortex may not undergo degeneration but rather develop with a reduced axonal arborization and complexity.

To evaluate the extent of noradrenergic signaling impairment in ALS mouse models, we ran quantitative polymerase chain reaction (qPCR) and Western blot analyses on microdissected motor cortices

Table 1. Clinical characteristics of the patients with sporadic ALS included in the rsEEG study. List of the patients included in the resting state EEG study and their age at recording, handedness, and main clinical features. LL, lower limb onset; B, bulbar onset; UL, upper limb onset. ALSFRS-r and UMN have arbitrary units. Disease duration is expressed in months. Progression rate represents the amount of lost points on the ALSFRS-r scale divided by the disease duration and is expressed in month^{-1}. Calculation of the mean progression rate of the group of patients with ALS allowed their segregation between fast (individual progression rate > mean progression rate) and slow progressors (individual progression rate < mean progression rate).

Patient	Age	Handedness	Site of onset	Disease duration	ALS-FRSR	Progression rate	Defined progression rate	UMN score
ALS 1	73	R	LL	60	37	0.183	Slow	0
ALS 2	62	L	B	36	34	0.389	Slow	3
ALS 3	63	R	LL	18	41	0.389	Slow	2
ALS 4	52	R	LL	45	36	0.267	Slow	3
ALS 5	45	R	UL	10	44	0.400	Slow	2
ALS 6	63	L	LL	15	44	0.267	Slow	3
ALS 7	41	R	UL	14	43	0.357	Slow	2
ALS 8	70	L	UL	36	40	0.222	Slow	0
ALS 9	80	R	LL	15	42	0.400	Slow	0
ALS 10	66	R	UL	8	36	1.500	Fast	2
ALS 11	74	R	B	8	34	1.750	Fast	3
ALS 12	77	R	LL	8	43	0.625	Fast	0
ALS 13	61	R	LL	76	41	0.092	Slow	4
ALS 14	72	R	LL	37	34	0.378	Slow	2
ALS 15	29	R	UL	22	38	0.455	Fast	3
ALS 16	73	R	B	11	43	0.455	Fast	3
ALS 17	67	R	B	6	47	0.167	Slow	3
ALS 18	59	R	LL	3	40	2.667	Fast	0
ALS 19	52	R	B	43	39	0.209	Slow	3
ALS 20	46	R	UL	31	35	0.419	Fast	3
ALS 21	68	R	UL	20	47	0.050	Slow	1
ALS 22	68	R	LL	9	40	0.889	Fast	0
ALS 23	42	R	UP	7	43	0.714	Fast	2
ALS 24	57	R	UP	9	35	1.444	Fast	3
ALS 25	61	R	LL	8	40	1.000	Fast	4
ALS 26	52	R	LL	7	38	1.429	Fast	4

and performed immunofluorescence experiments to assess the expression of adrenergic receptors and NA degradation enzymes (Fig. 5, D to L, and fig. S8). Expression of beta 1 (fig. S8A) and alpha 2C (fig. S8B) adrenergic receptor genes was unaltered in both mouse lines. Contrastingly, alpha 2A and alpha 2B adrenergic receptor mRNA expression was decreased in the motor cortex of *Sod1*^{G86R} mice compared with WT (genotype effect in mixed-effect analysis: $P = 0.0002$ for *Adra2a* and $P < 0.0001$ for *Adra2b*; Fig. 5, D and E) and of *Fus*$^{\Delta NLS/+}$ mice compared with WT ($P = 0.0112$ for *Adra2a* and $P = 0.0042$ for *Adra2b* in two-sided *t* test; Fig. 5, D and E). Beta 2 adrenergic receptor gene expression was also decreased in *Sod1*^{G86R} ($P = 0.0038$) but unchanged in *Fus*$^{\Delta NLS/+}$ mice compared to their respective WT littermates (Fig. 5F). Western blot analyses revealed decreased protein expression of alpha 2B and beta 2 adrenoreceptors in *Fus*$^{\Delta NLS/+}$ mice ($P = 0.0336$ for alpha 2B and $P = 0.0152$ for beta 2; Fig. 5, H and I, and fig. S8, D and E) but not in *Sod1*^{G86R} mice. Immunofluorescence further allowed us to reveal and quantify the expression of these receptors in neuronal subpopulations of interest within cortical layer V, namely, COUP-TF-interacting protein 2 (CTIP2)–positive excitatory neurons and PV- and somatostatin (SST)–positive interneurons (Fig. 5, J to L, and fig. S8, F and G). Alpha 2A was overall found to be enriched in CTIP2-positive compared with PV- and SST-positive neurons, and its protein expression was significantly decreased in CTIP2-positive neurons of 60-day-old *Sod1*^{G86R} mice compared with their WT littermates ($P = 0.0004$ in multiple comparisons test; Fig. 5J). Alpha 2B and alpha 2C were found to be enriched in CTIP2- and SST-positive neurons compared with PV-positive neurons, but their expression by these neuronal subpopulations was not affected in *Sod1*^{G86R} animals (Fig. 5J and fig. S8F). Noradrenergic impairment was further indicated by the differential expression of genes encoding NA degradation enzymes: monoamine oxidases A and B and catechol-*O*-methyltransferase (*Maoa*, *Maob*, and *Comt*). *Maoa* expression was unchanged (fig. S8G), *Maob* expression was significantly increased in *Sod1*^{G86R} animals (genotype effect: $P = 0.0106$ in mixed-effect analysis) but not in *Fus*$^{\Delta NLS/+}$ animals ($P = 0.5319$ in two-sided *t*

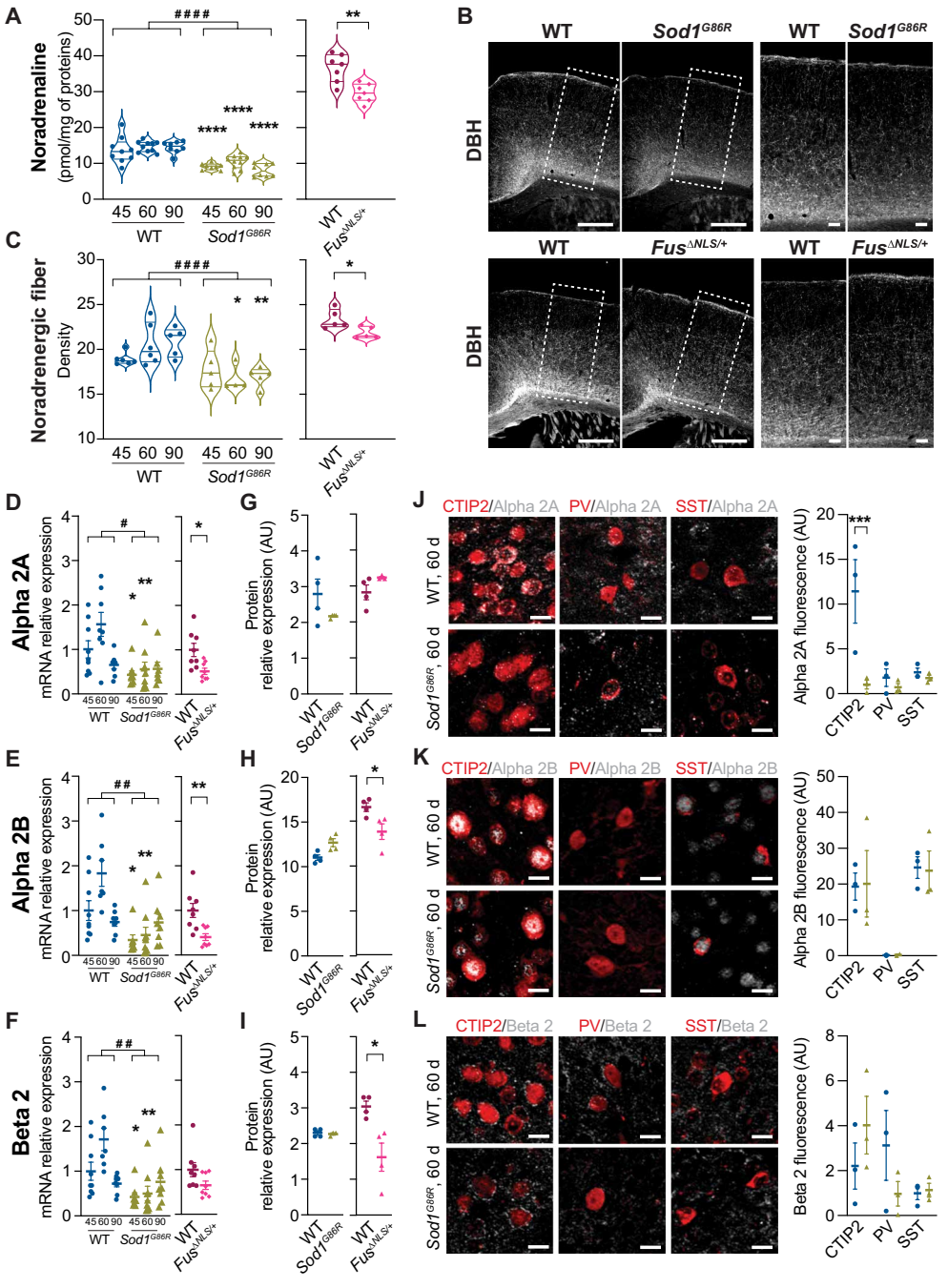

Fig. 5. The motor cortex of *Sod1*^{G86R} and *Fus*$^{\Delta NLS/+}$ mice exhibits altered NA homeostasis. (**A**) NA concentration measured by LC-MS in the motor cortex of 45-, 60-, and 90-day-old *Sod1*^{G86R} and 4-month-old *Fus*$^{\Delta NLS/+}$ female mice and their respective controls ($n = 9$ WT and 8 *Sod1*^{G86R} at 45 days, 10 WT and 10 *Sod1*^{G86R} at 60 days, and 8 WT and 8 *Sod1*^{G86R} at 90 days; $n = 8$ WT and 8 *Fus*$^{\Delta NLS/+}$). (**B**) Representative images of the cerebral cortex of 90-day-old WT and *Sod1*^{G86R} mice and 4-month-old WT and *Fus*$^{\Delta NLS/+}$ mice after DBH immunolabeling. Scale bars, 500 and 100 μm in close-ups. (**C**) Quantifications of cortical DBH-positive noradrenergic fiber density in 45-, 60-, and 90-day-old *Sod1*^{G86R} female mice and controls and 4-month-old *Fus*$^{\Delta NLS/+}$ female mice and controls ($n = 6$ WT and 5 *Sod1*^{G86R} at 45 days, 6 WT and 4 *Sod1*^{G86R} at 60 days, and 5 WT and 5 *Sod1*^{G86R} at 90 days; $n = 5$ WT and 5 *Fus*$^{\Delta NLS/+}$). (**D** to **F**) Relative mRNA expression levels of *Adra2a*, *Adra2b*, and *Adrb2* in the motor cortex of 45-, 60-, and 90-day-old *Sod1*^{G86R} and 4-month-old *Fus*$^{\Delta NLS/+}$ female mice and their respective controls ($n = 9$ WT and 8 *Sod1*^{G86R} at 45 days, 8 WT and 8 *Sod1*^{G86R} at 60 days, and 8 WT and 8 *Sod1*^{G86R} at 90 days; $n = 8$ WT and 8 *Fus*$^{\Delta NLS/+}$). (**G** to **I**) Quantification of adrenergic receptors 2A, 2B, and B2 revealed by Western blot in motor cortex extracts from 90-day-old *Sod1*^{G86R} and 6-month-old *Fus*$^{\Delta NLS/+}$ mice and their respective controls ($n = 4$ female mice per group). (**J** to **L**) Representative images of the cerebral cortex (left) of 60-day-old WT and *Sod1*^{G86R} mice immunolabeling to reveal adrenergic receptors 2A (J), 2B (K), and B2 (L) (white) along with CTIP2-, PV-, and SST-positive neurons (red) (scale bars, 10 μm) and quantification of the receptor expression (right) based on fluorescence in the corresponding graphs to the left ($n = 3$ female mice per group). *Sod1*^{G86R} mRNA samples were analyzed by two-way ANOVA followed by multiple comparisons test; *Fus*$^{\Delta NLS/+}$ mRNA samples and protein expression for *Sod1*^{G86R} and *Fus*$^{\Delta NLS/+}$ were analyzed by two-sided unpaired Student's *t* test. #$P < 0.05$; ##$P < 0.01$; ####$P < 0.0001$ for genotype effect in two-way ANOVA and *$P < 0.05$; **$P < 0.01$; ***$P < 0.001$; ****$P < 0.0001$ in pairwise comparisons with age-matched WT controls. AU, arbitrary units.

test; fig. S8H), and *Comt* expression was unaffected in *Sod1*^{G86R} animals (genotype effect: $P = 0.2094$ in mixed-effect analysis) but significantly increased in *Fus*$^{\Delta NLS/+}$ animals ($P = 0.0131$ in two-sided *t* test; fig. S8I), suggesting different regulatory mechanisms affecting each gene in each mouse line. Together, the data indicate that noradrenergic signaling is impaired in the motor cortex of both *Sod1*^{G86R} and *Fus*$^{\Delta NLS/+}$ mouse models of ALS, reflected in decreased NA concentration, decreased noradrenergic innervation, and altered expression of noradrenergic receptors and degradation enzymes.

Behaving *SOD1*^{G93A} and *Fus*$^{\Delta NLS/+}$ mice display compromised NA release in the primary motor cortex

We next asked whether NA release was also affected in vivo. Because the activity of corticopetal axonal NA projections strongly correlates with locomotion (*45*, *46*), we probed running-associated NA release by means of in vivo two-photon imaging in a third ALS mouse model, *SOD1*^{G93A} mice, as well as in *Fus*$^{\Delta NLS/+}$mice and their respective WT littermates, while animals were head-fixed moving on a spherical treadmill (Fig. 6A and fig. S9). Expression of the genetically

encoded NA indicator GPCR activation-based norepinephrine (GRAB_NE1m) was achieved through AAV transduction. We observed an increase in fluorescence, corresponding to NA release, associated with running onsets in the primary motor cortex layer II/III (Fig. 6, B and C, and fig. S9, A to C). When comparing the locomotion-associated signal in early symptomatic $SOD1^{G93A}$ (90 days old) and $Fus^{\Delta NLS/+}$ (4 months old) mice with WT controls, we found a strong reduction within −0.5 to +1.5 s of running onset [11.18 ± 2.83 in WT versus −0.95 ± 2.42 $SOD1^{G93A}$, $P = 0.0023$ (Fig. 6D) and 9.88 ± 3.25 in WT versus −4.53 ± 2.58 $Fus^{\Delta NLS/+}$, $P = 0.0084$, Wilcoxon rank sum test for the area under the curve from −0.5 to 1.5 s with respect to locomotion onset (fig. S9D)], illustrating a strong reduction of NA release. To rule out the contribution of running velocities, we computed the tuning curves of this response, by measuring the fluorescence intensity change as a function of average running speed within a 3-s window after running onset. The tuning curve revealed a positive linear relationship of fluorescence intensity and running velocity in WT mice ($y = 0.48x + 0.01$, $R^2 = 0.91$, slope $P = 0.012$; Fig. 6E). In $SOD1^{G93A}$ mice, however, there was not only a strong overall reduction in locomotion-associated NA release, but, moreover, the velocity-dependent increase in fluorescence was greatly diminished ($y = 0.13x + 0.003$, $R^2 = 0.482$, slope $P = 0.19$, difference in slope difference between WT and $SOD1^{G93A}$ $P = 0.0148$; Fig. 6E). A similar reduction was found in $Fus^{\Delta NLS/+}$ mice (linear fit of the maximum values within −0.5 to 1.5 s of the running onset in the different velocity bins in WT: $y = 0.638x + 0.004$, $R^2 = 0.862$ and $Fus^{\Delta NLS/+}$ mice: $y = 0.219x + 0.005$, $R^2 = 0.313$, intercept difference between WT and $Fus^{\Delta NLS/+}$ $P = 0.0462$, one-way ANOVA; fig. S9E). Because NA release could potentially also occur with a temporal offset within a given brain area, we also assessed the synchrony of NA release within a given field of view by computing the pairwise correlation coefficient between individual regions of interest (Fig. 6F). This analysis revealed no significant difference between WT and $SOD1^{G93A}$ mice ($P = 0.64$; Fig. 6G). Together, our data show that NA release is strongly impaired in M1 of $SOD1^{G93A}$ and $Fus^{\Delta NLS/+}$ mice.

Patients with sporadic ALS present with altered cortical noradrenergic signaling

To assess the relevance of our findings in patients with ALS, we conducted LC-MS analyses on postmortem motor cortex, LC, and spinal cord from sporadic patients and controls (table S1) and performed transcriptomic analyses on postmortem motor and prefrontal cortices from sporadic patients and controls. LC-MS analyses revealed a significant decrease of NA in the motor cortex and LC of patients compared with healthy controls ($P = 0.039$ and $P = 0.01$, respectively; Fig. 7A) but not in the spinal cord (Fig. 7A). NA concentrations in postmortem samples did not correlate with the age of death, neither among the control nor among the samples from

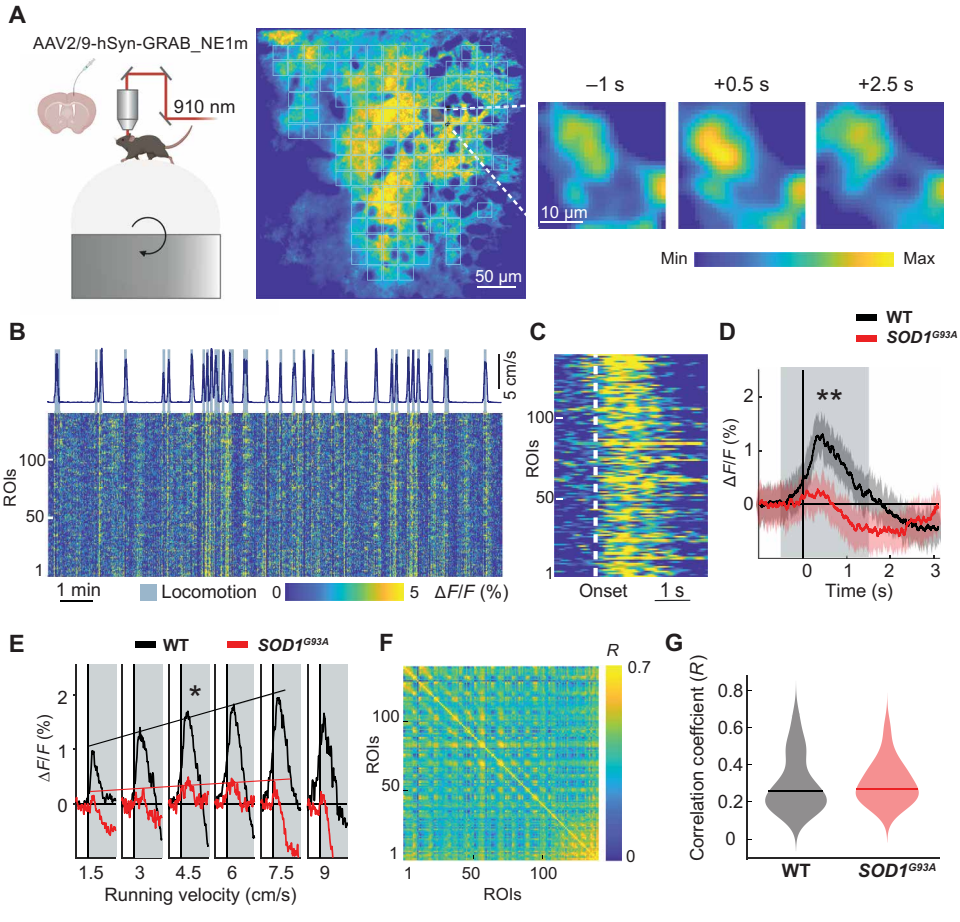

Fig. 6. Release of NA in behaving mice is strongly diminished in $SOD1^{G93A}$ mice. (**A**) NA release associated with locomotion was assessed by in vivo two-photon imaging of the AAV-mediated expression of the NA indicator GRAB_NE1m in head-fixed mice running on spherical treadmill. Mean projection of an example field of view (FOV) from a WT mouse. Superimposed grid demonstrates location and size of regions of interest (ROIs). Representative ROI referenced by time with respect to locomotion onset shown on the right. (**B**) Heatmap of fluorescent traces of all ROIs in an example FOV of a WT mouse shown in (A) across the entire recording session referenced by running speed (blue trace on top) and binary running epochs (blue area). (**C**) Averaged running-associated response of each ROI for the same FOV shown in (B). (**D**) Average population response to locomotion onset of all FOVs in WT (black) and $SOD1^{G93A}$ mice (red) [$P = 0.0023$, two-sided Student's t test for the area under the curve (gray area), WT: 20 FOV, two male and two female mice; $SOD1^{G93A}$: 20 FOV, two male and three female mice]. (**E**) Speed-dependent tuning curve of the locomotion-associated NA release (maximum value within −0.5 to 1.5 s of running onset, gray area) in WT ($y = 0.48x + 0.01$, $R^2 = 0.91$, slope $P = 0.012$, two-sided Student's t test) and $SOD1^{G93A}$ mice ($y = 0.13x + 0.003$, $R^2 = 0.482$, slope $P = 0.19$, slope difference between WT and $SOD1^{G93A}$ $P = 0.0148$, two-sided unpaired Student's t test). (**F**) Correlogram depicting pairwise correlations (Pearson's correlation coefficient) of individual ROIs in the same FOV shown in (B) and (C). (**G**) Pairwise ROI correlations do not differ between WT and $SOD1^{G93A}$ mice. *$P < 0.05$ and **$P < 0.01$.

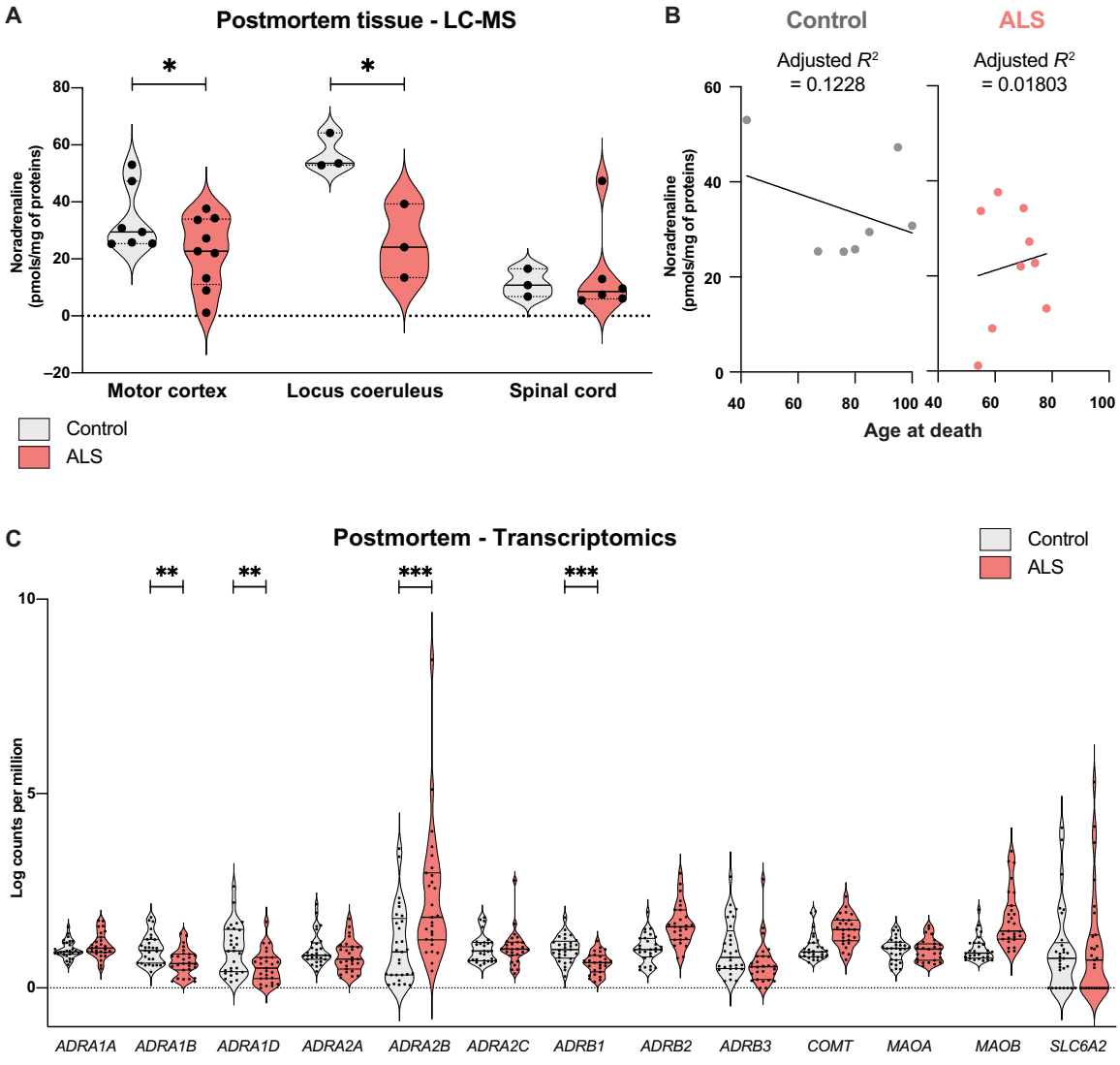

Fig. 7. Postmortem motor cortex and LC from patients with ALS display decreased NA concentration, along with altered expression of genes involved in noradrenegeric signaling. (**A**) LC-MS quantification of NA in the postmortem motor cortex, LC, and spinal cord of patients with ALS (coral) and age-matched healthy controls (gray). Motor cortex: $n = 7$ healthy controls, 9 patients with ALS; LC: $n = 3$ healthy controls, 3 patients with ALS; spinal cord: $n = 3$ healthy controls, 6 patients with ALS. One-sided unpaired Student's t test. $^*P < 0.05$; $^{**}P < 0.01$. (**B**) Correlation between NA in postmortem motor cortices from healthy controls (left, gray) or patients with ALS (right, coral) and their age at death. (**C**) Relative mRNA expression of genes involved in noradrenergic signaling in the postmortem motor and frontal cortices of patients with ALS (coral) and age-matched healthy controls (gray). $n = 29$ healthy controls and 27 patients with ALS. Differential gene expression analysis; **FDR < 0.01; ***FDR < 0.001.

patients (Pearson correlation, $P = 0.4409$, $R^2 = 0.1228$ for controls and $P = 0.7306$, $R^2 = 0.01803$ for patients; Fig. 7B and table S1). Glutamate concentrations were unaltered in the motor cortex and spinal cord but significantly decreased in the LC of patients with ALS compared with controls ($P = 0.003$; fig. S10A). GABA concentrations were significantly decreased in the motor cortex and LC of patients compared with healthy individuals ($P = 0.034$ and 0.0095, respectively; fig. S10B). Last, as expected, serotonin concentrations were decreased in the motor cortex of patients compared with controls ($P = 0.0078$; fig. S10C) but were not significantly altered in the spinal cord of patients. Thus, the LC-MS data indicate that patients with ALS present with decreased NA in the motor cortex and LC, along with decreased GABA in these same structures and decreased glutamate in the LC, suggesting multifaceted alterations of proper circuit function within these brain regions. Transcriptomic analyses revealed significantly decreased expression of *ADRA1B* [false discovery rate (FDR) = 0.0020], *ADRA1D*, (FDR = 0.00638), *ADRB1* (FDR = 0.00014), and *ADRA2B* (FDR = 0.00010; Fig. 7C). Together, LC-MS and transcriptomic data indicate that noradrenergic homeostasis is also altered in the motor cortex of sporadic patients.

Experimental modulation of noradrenergic homeostasis alters cortical circuit function in WT and *Sod1*^{G86R} mice

To test whether impaired NA homeostasis could contribute to cortical hyperexcitability and broader network dysfunction, we first experimentally triggered cortical NA depletion in WT mice, taking

advantage of the *N*-(2-chloroethyl)-*N*-ethyl-2-bromobenzylamine (DSP-4) neurotoxin that selectively affects noradrenergic neurons of the LC (Fig. 8, A to E, and fig. S11) (*47*). As expected, DSP-4 treatment selectively decreased cortical NA ($P < 0.0001$; fig. S11A) without affecting the concentrations of glutamate, GABA, serotonin, and dopamine (fig. S11A). A first cohort of WT mice underwent a PTZ susceptibility test, before and 8 days after DSP-4 injection (Fig. 8A). DSP-4 treatment significantly increased PTZ susceptibility by 62.03 ± 8.26% in these mice ($P = 0.0005$; Fig. 8, B and C). A second cohort of WT mice underwent T-HG PAC measurements during REM sleep, before and 48 hours after DSP-4 injection (Fig. 8D). T-HG PAC was significantly decreased in mice upon DSP-4 administration compared with the pretreatment condition ($P = 0.0048$; Fig. 8E), although theta, high gamma, and total power remained unchanged (fig. S11, B to D). DSP-4 administration also induced decreased T-LG PAC during REM sleep ($P = 0.0098$; fig. S11F) that might arise partly from overall decreased low gamma power ($P = 0.0282$; fig. S11E). Together, the data indicate that experimentally induced cortical NA depletion is sufficient to trigger cortical hyperexcitability as manifested by increased PTZ susceptibility and decreased T-HG PAC. This phenotype is reminiscent of that observed in the *Sod1*^{G86R} and *Fus*$^{\Delta NLS/+}$ mouse models of ALS.

Second, we tested whether experimental supplementation of NA in *Sod1*^{G86R} mice would be sufficient to revert cortical hyperexcitability (Fig. 8, F and G). We used a combination of L-threo 3,4-dihydroxyphenylserine (L-DOPS) and benserazide. L-DOPS is a synthetic precursor of NA that is metabolized to NA by the aromatic acid decarboxylases. Benserazide is an inhibitor of the aromatic acid decarboxylases that does not cross the blood-brain barrier. Thus, the combination of L-DOPS and benserazide allows us to increase NA concentration selectively in the central nervous system (*48*). We failed to detect an increase of NA in L-DOPS + benserazide-treated animals, compared to saline-injected animals, all harvested 12 hours postinjection, independent of their genotype (fig. S12A), which likely arises from the very short effect of L-DOPS on NA concentration in the central nervous system that peaks 5 hours postinjection (*48*). Glutamate, GABA, and serotonin remained unaffected (fig. S12, B to D). T-HG PAC was significantly increased in *Sod1*^{G86R} animals ($P = 0.0290$ for *Sod1*^{G86R}; Fig. 8G), without any significant effect on theta, high gamma, and total powers (fig. S12, E to G). L-DOPS + benserazide injection had no effect on the T-HG PAC in WT animals (Fig. 8G) but significantly increased both theta and total powers in these animals ($P = 0.0060$ and $P = 0.0039$, respectively; fig. S12, E and G).

To finally test whether cortical hyperexcitability could be reduced over a longer period of time, we selected yohimbine, an alpha 2 antagonist described to increase synaptic NA concentration by blocking presynaptic alpha 2A adrenoreceptors that are responsible for the negative feedback on noradrenergic release *(49)*. Chronic in vivo two-photon imaging in 4-month-old *Fus*$^{\Delta NLS/+}$mice and their WT littermates revealed a significant increase in NA release after 10 days of yohimbine treatment (6 mg/kg per day) in WT control and, to a lesser degree, also in *Fus*$^{\Delta NLS/+}$mice (fold change in WT: baseline versus day 10, 1.14 + [1.04 1.24], $P = 0.0027$; day 2 versus day 10, $P = 0.0047$; *Fus*$^{\Delta NLS/+}$: baseline versus day 10, 1.19 + [0.97 1.29], data are median + 95% confidence interval, $P = 0.022$; day 2 versus day 10, $P = 0.092$, all Wilcoxon rank sum tests; fig. S13, A to F). Chronic imaging in saline-treated mice instead did not reveal any increase of the fluorescent signal (fig. S13G). T-HG PAC was then assessed in WT and *Sod1*^{G86R} mice during REM sleep, before (45 days) and every 10 days upon daily injection of yohimbine (Fig. 8H). Yohimbine significantly increased T-HG PAC in *Sod1*^{G86R} mice for at least 20 days ($P = 0.0195$ and $P = 0.0052$ between baseline and 10 and 20 days posttreatment, respectively, in mixed-effects analysis followed by multiple comparisons test; Fig. 8I), meaning until at least 65 days of age. Last, we tested the consequences that a chronic yohimbine treatment, initiated at the age of 60 days, has on disease onset, motor phenotype, and survival in *Sod1*^{G86R} mice (fig. S14). The results indicate that the treatment did not modify the onset, survival, or symptom severity (fig. S14). This lack of efficiency may be attributed to the temporally limited effect of yohimbine on cortical hyperexcitability.

Together, these experiments indicate that impaired cortical NA homeostasis contributes to cortical hyperexcitability and motor cortex network dysfunction in ALS. Follow-up studies will be needed to identify a drug or method to permanently correct NA impairment and cortical hyperexcitability in mice before assessing the consequences on symptom onset, progression, and survival.

DISCUSSION

Cortical hyperexcitability has been so far detected in patients with ALS using ppTMS protocols (*5*). The method, however, falls short in cases of advanced UMN and LMN dysfunction and degeneration that prevent faithful measurements at the level of the muscles. We thus sought to provide proof of principle experiments that cortical hyperexcitability can be assessed by means of noninvasive EEG measurements, independent of the integrity of the corticospinal pathway and neuro-muscular connectivity.

We reasoned that cortical circuit E/I imbalance could be approached in rodents by combining ECoG with other established means, such as the sensitivity to the $GABA_A$ antagonist PTZ (*32*) and theta-gamma PAC (*11, 12*). Compared with their respective WT littermates, *Sod1*^{G86R} and *Fus*$^{\Delta NLS/+}$ mice displayed increased sensitivity to PTZ, indicative of a hyperexcitable network. The underlying molecular and cellular mechanisms of this might, however, be manifold, including dysfunction of GABAergic inhibitory neurons as well as enhanced excitability of pyramidal neurons (*6, 7*). PTZ is commonly used to probe for an epileptic phenotype in models of CNS disorders, including AD (*33*), given that about 10% of AD cases display epileptic discharges or seizures (*50*). To the best of our knowledge, such a comorbidity has never been described in ALS, and no common genetic risk has been reported *(51)*. Accordingly, neither *Sod1*^{G86R} nor *Fus*$^{\Delta NLS/+}$ animals displayed any convulsive seizures upon the application of PTZ (30 mg/kg), a dose that otherwise readily triggers epileptic seizures in animal models of tauopathy or FTD (*52, 53*). Thus, our results suggest that *Sod1*^{G86R} and *Fus*$^{\Delta NLS/+}$ mice recapitulate cortical hyperexcitability.

Cortical E/I imbalance can further be assessed in vivo by EEG/ECoG recordings combined with PAC analyses. PAC has been reported both in human and rodent brains, between different slow and fast frequency bands, and is modulated in a task- and disease-dependent manner (*54*). Studies conducted in the motor cortex of rats and humans indicate strong theta-gamma coupling in this area (*38–40*). In addition, EEG recordings in patients with chronic hemiparetic stroke demonstrated that theta-gamma coupling was increased during brain-computer interface rehabilitation therapy (*39*). The effect was selectively observed in the C_3 and C_4 channels and

selective to theta-gamma PAC (as opposed to alpha-gamma and beta-gamma) (*39*). All these data prompted us to assess theta-gamma PAC in ALS mouse models and patients over the sensory-motor areas. We report here that two mouse models of ALS and FTD, *Sod1*^{G86R} and *Fus*$^{\Delta NLS/+}$ mice, present with decreased theta-gamma PAC, already during presymptomatic stages and throughout their entire lifetime. Together with their increased susceptibility to PTZ, our data suggest that preclinical models of the disease display cortical dysfunction reminiscent of cortical hyperexcitability. These findings are of translational relevance, because we also found decreased theta-gamma PAC in patients with ALS. Compromised PAC was not due to changes in absolute power, as described in late-stage ALS, when patients enter a locked-in state (*55, 56*). We found more pronounced changes in PAC during REM sleep compared with wakefulness in the two mouse models of the disease. In patients with ALS, however, the detection of REM sleep episodes is hampered by progressive paralysis, affecting also eye movements (*55*), which complicates this assessment. We thus opted to perform EEG recordings in awake patients. Decreased theta-gamma PAC was most prominently detected over the left motor area, which could be explained by the fact that most of our participants were right-handed. Investigations of larger cohorts, including left-handed participants, will, however, be needed to address this aspect in more detail. Decreased theta-gamma PAC did not correlate with UMN impairment, indicating its potential to reveal cortical network dysfunction independent of UMN damage, noticeably heterogeneous across patients (*1*). Decreased theta-gamma PAC correlated instead with disease progression, strongly encouraging future studies in patients

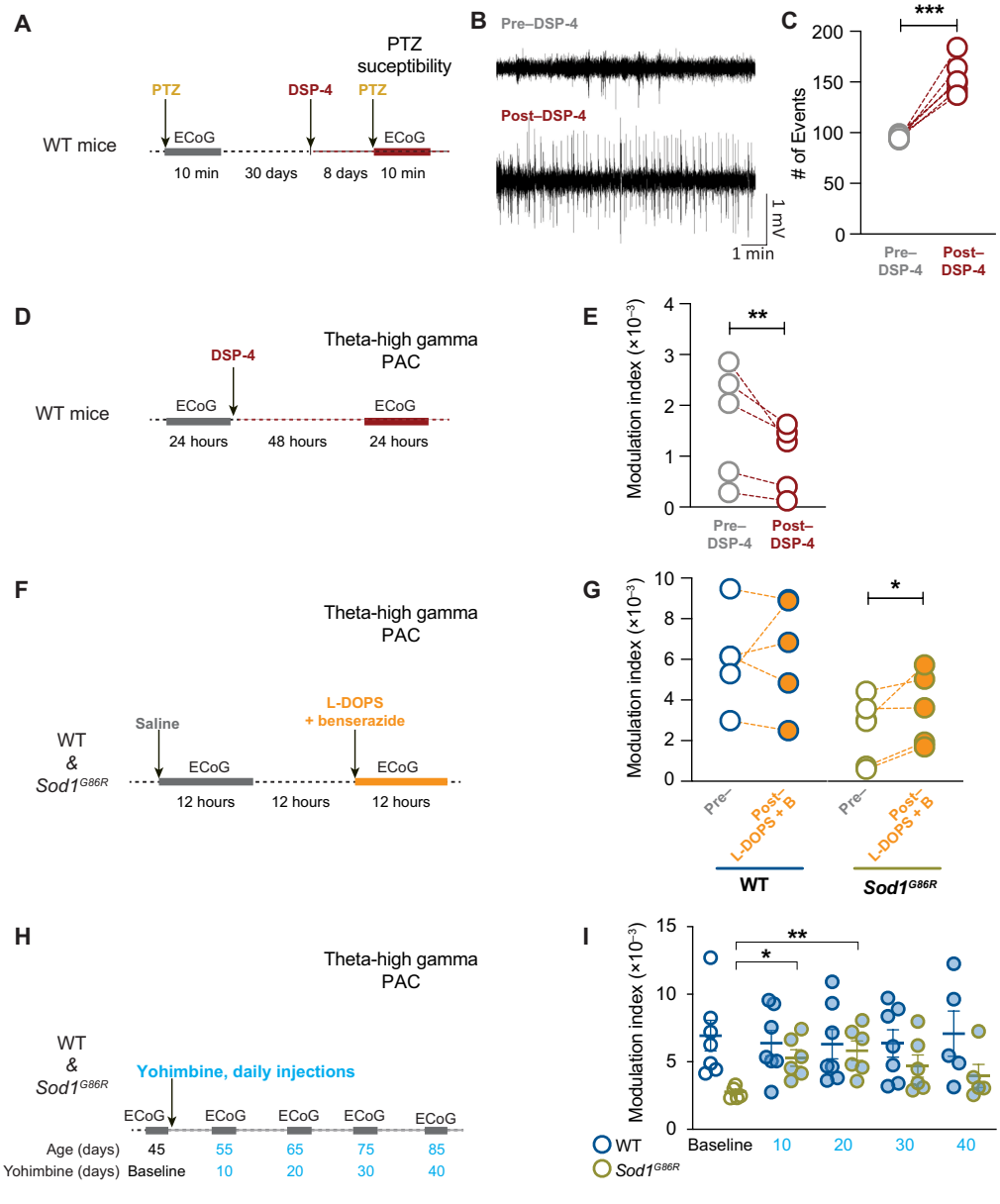

Fig. 8. NA critically regulates cortical hyperexcitability and theta-gamma PAC. (**A**) Schematic representation of the experimental paradigm: PTZ was administered in WT mice before each ECoG recording, and two EcoG recordings were performed 38 days apart from each other, before and 8 days after DSP-4 administration to induce noradrenergic fiber degeneration and cortical NA depletion. (**B**) Representative ECoG traces after a single injection of PTZ of WT animals before or after DSP-4 administration. (**C**) Before-after graph representing the number of epileptiform-like events triggered by PTZ before and after DSP-4 administration ($n = 4$ WT female mice); two-sided paired Student's t test; $^{***}P < 0.001$. (**D**) Schematic representation of the experimental paradigm: Two EcoG recordings were performed 48 hours apart from each other, before and after DSP-4 administration. (**E**) Before-after graph representing the MI of T-HG PAC during REM sleep before and after DSP-4 administration ($n = 5$ WT animals); two-sided paired Student's t test; $^{**}P < 0.01$. (**F**) Schematic representation of the experimental paradigm: Two EcoG recordings were performed 12 hours apart from each other, before and after L-DOPS and benserazide administration. (**G**) Before-after graph representing the MI of T-HG PAC during REM sleep before and after L-DOPS and Benserazide administration in *Sod1*^{G86R} mice and their WT littermates ($n = 4$ WT and 5 *Sod1*^{G86R} female mice); two-sided paired Student's t test; $^{*}P < 0.05$. (**H**) Schematic representation of the experimental paradigm: Five EcoG recordings were performed 10 days apart from each other, before and during daily yohimbine administration. (**I**) Graph representing the MI of T-HG PAC during REM sleep before and after yohimbine administration in *Sod1*^{G86R} mice and their WT littermates ($n = 7$ WT and 6 *Sod1*^{G86R} female mice); two-way ANOVA followed by multiple comparisons test; $^{*}P < 0.05$; $^{**}P < 0.01$; in pairwise comparisons between untreated and treated *Sod1*^{G86R} mice.

with familial ALS and presymptomatic mutation carriers to determine whether it has the potential to become an indicator of early cortical impairment and disease stage in ALS, potentially improving diagnosis and prognosis.

Taking advantage of comparable theta-gamma PAC impairment in patients with sporadic ALS and mouse models, we strove to gain insight into its cellular and molecular mechanisms. We reasoned that altered E/I balance could at least in part rely on neuromodulatory alterations (*23, 57*). We observed a mild decrease of glutamate in the motor cortex of *Sod1*^{G86R} mice but not in that of *Fus*$^{\Delta NLS/+}$ mice or in patients with ALS. GABA was unaltered in the motor cortex of the two mouse models but decreased in patients, which could reflect a greater impairment of the cortical GABAergic system in patients with ALS compared with mouse models. We further confirmed a decrease of serotonin in the motor cortex of patients with ALS and *Sod1*^{G86R} mice, in agreement with previous studies (*24, 25*). Most critically, we provide evidence for decreased concentration of NA in the motor cortex of patients with sporadic ALS, which was conserved in the *Sod1*^{G86R}, *Fus*$^{\Delta NLS/+}$, and *SOD1*^{G93A} mouse models of the disease. Decreased NA concentration was also observed in the LC of patients with ALS but not in spinal cord. In the LC of patients with ALS, we also found decreased glutamate and GABA that may reflect a global functional impairment of this nucleus and could potentially also underlie the noradrenergic deficits observed in both the LC itself and the motor cortex of patients. Former HPLC studies conducted on spinal cord homogenates from patients with ALS revealed either decreased (*58*) or instead increased (*59*) concentration of NA. In the cerebrospinal fluid (CSF) of patients with ALS, however, NA was found to be increased (*60*–*62*), which may reflect a dysfunction of the central noradrenergic system. Decreased NA concentration has so far been mostly reported in AD and PD, in which cases it was linked to an early degeneration of the LC (*27, 28*). Whereas histological defects, such as neuronal loss and neurofibrillary tangles, were observed in the LC of patients with ALS (*63, 64*), typical pTDP-43 pathology was notably absent (*65*). This, however, does not per se rule out an impairment of noradrenergic neurons. Quantification of TH-positive neurons in the LC of *Sod1*^{G86R} and *Fus*$^{\Delta NLS/+}$ mice, along with retrograde labeling of LC neurons projecting to the motor cortex in *Sod1*^{G86R} mice, excluded the hypothesis of major noradrenergic neuron degeneration in these animals. Instead, the decreased noradrenergic fiber density in the motor cortex of *Sod1*^{G86R} and *Fus*$^{\Delta NLS/+}$ mice, along with the increased expression of *Maob* and *Comt* in *Sod1*^{G86R} and *Fus*$^{\Delta NLS/+}$ mice, respectively, is likely to contribute to NA deficiency in this region. One can speculate that decreased NA fiber density or altered LC function may similarly contribute to decreased NA release seen in behaving *SOD1*^{G93A} and *Fus*$^{\Delta NLS/+}$ animals. NA release is strongly associated with wakefulness, and NA neurons of the LC are nearly silent during REM sleep, a phenomenon that is at least partly attributed to the strong control of the suprachiasmatic nucleus, the central pacemaker of the circadian timing system, over the LC [reviewed in (*66*)]. It is thus tempting to speculate that NA release during wakefulness, even if diminished in ALS, may partially dampen the otherwise observed cortical hyperexcitability and that the absence of NA during REM sleep would further potentiate cortical hyperexcitability. This might explain why theta-gamma PAC deficits are more prominent during REM sleep than during active wakefulness in ALS mouse models. In sum, the mechanisms driving the dysfunction or degeneration of NA neurons in the LC as well as reduced NA innervation and release in cortical areas of patients with ALS and mouse models warrant further scrutiny.

Previous reports have also shown that NA decreases excitation by lowering AMPA-mediated glutamatergic transmission through Alpha 1 and Alpha 2 adrenoreceptors and increases the synaptic responses mediated by $GABA_A$ receptors (*67*). Accordingly, LC stimulation was demonstrated to protect epileptic patients from seizures (*68*–*70*). In addition, both pharmacologically and genetically induced NA deficiency was demonstrated to increase CNS excitability in mice, with increased susceptibility to various convulsant agents and increased c-Fos expression in the neocortex, hippocampus, and amygdala (*71, 72*). In line with these reports, we also found an increase in cortical excitability assessed upon PTZ challenge, as well as a decrease in theta-gamma PAC in WT mice treated with DSP-4. Overall, these studies indicate that NA can exert a global inhibitory effect on cortical activity and support the notion that NA deficiency contributes to cortical hyperexcitability in ALS. We also show that both NA supplementation and Alpha 2 blockage in *Sod1*^{G86R} mice can rescue the PAC deficit at least transiently. These data indicate that NA deficiency contributes to cortical activity dysregulation and that increasing cortical NA can help restore it. We attempted to chronically restore NA signaling using yohimbine, which, however, only exerted a transient effect on cortical excitability that might explain the absence of beneficial effect on disease onset and progression. Additional strategies to maintain NA homeostasis in a more sustained manner will be needed to address this important question. It is noteworthy that numerous drugs exist that increase central NA with indications for attention deficit disorder, narcolepsy, and excessive sleepiness, such as amphetamines, atomoxetine, methylphenidate, or solriamfetol (*73*); or anxiety and depression, such as serotonin and NA reuptake inhibitors, antagonists of inhibitory presynaptic serotonin, and NA receptors, or inhibition of the monoamine oxidase (*74*). These represent many possible candidates to restore central NA homeostasis in ALS mouse models and assess the consequences on disease onset and progression. The risk of depression is increased in patients with ALS (*75*), in which case antidepressants can be prescribed. However, with the exception of rasagiline (*76*), a MAO-B inhibitor, such drugs have, to our knowledge, never been directly assessed for their ability to slow down disease progression in patients with ALS. Apart from their effect on the CNS, it is worth mentioning that guanabenz, an alpha 2 agonist, and clenbuterol, a beta 2 agonist, have been tested in patients with ALS for their ability to prevent misfolded protein accumulation or to protect muscle mass and strength, respectively, and provided encouraging first results (*77, 78*). Investigating the effect of these drugs on cortical excitability would be of particular interest in the context of our results.

There are some limitations to our study, including the methodology we have used to assess PAC in rsEGG, which was done over a period of 5 min. Given that PAC is not homogeneous over time, longer recording times or further segmentation of the recordings may in the future reduce the variability of the MI and unravel even more pronounced and robust PAC deficits in patients. In addition, although patients' MI negatively correlated with disease progression, it is noteworthy that the progression rate was calculated from a single ALSFRS-r measurement. Future studies will be needed to include several EEG recordings and corresponding ALSFRS-r assessments to better evaluate how PAC deficits reflect disease progression. Another limitation lies in human NA measurements that were

performed on postmortem tissues and not from the same individuals who underwent EEG recording. Therefore, correlation between NA deficits and PAC impairment was not possible, and future studies will be needed to address this limitation potentially through longitudinal NA measurements in the CSF.

Together, we here show that compromised theta-gamma PAC is present in patients in ALS and mouse models of the disease and reflects cortical hyperexcitability, which in turn is at least in part driven by NA deficiency. Although the exact mechanisms through which NA alterations contribute to cortical hyperexcitability remain to be determined, the central noradrenegric system offers a promising pathway to modulate cortical network dysfunction in ALS.

MATERIALS AND METHODS

Study design

The aims of this study were (i) to test whether cortical hyperexcitability in mouse models and patients with ALS could manifest in EEG and ECoG as altered theta-gamma coupling and (ii) to gain insight into its cellular and molecular origins. ECoG in the *Sod1*^{G86R} and *Fus*$^{\Delta NLS/+}$ ALS mouse models was performed, and theta-gamma PAC was characterized and compared with healthy control mice. Sample size was estimated on the basis of former studies in rodents (*17*). In vivo two-photon imaging in behaving mice, LC-MS, histology, and transcriptomics were used to characterize changes in NA signaling in ALS mouse models. Sample size was estimated on the basis of former studies (*20*). All mouse experiments were approved by the local ethics committee of Strasbourg University [Comité d'éthique en matière d'expérimentation animale de Strasbourg (CREMEAS), authorization #12138-2017111016579993 v3] and the government of Upper Bavaria. Experiments on presymptomatic animals were blinded. EEG data from 26 patients with ALS and 26 matched healthy controls were obtained. EEG procedures conformed to the lasted revision of the Code of Ethics of the World Medical Association (Declaration of Helsinki) and were approved by the ethics committee of Inserm (protocol C17-70) and by the national ethical authorities (CPP Ouest II Angers, no. 18.07.11.57804 2018/58; RCB 2018) and recorded in public register (ClinicalTrials.gov, NCT03694132). Each participant provided their written informed consent. The PAC analysis in patients is part of a more extensive study primarily focused on investigating the integration of sensory feedback at the cerebral level in ALS, using EEG, magnetoencephalography (MEG), and magnetic resonance imaging. Using a 5% alpha risk, we determined a sample size for a *t* test and its corresponding power. The statistical analysis yielded a projected sample size of 26 individuals, with a test power of 75%. Recordings on humans were not blinded because of the motor phenotypes of patients with ALS. LC-MS on postmortem tissue samples from 9 patients with sporadic ALS and 7 healthy controls and transcriptomics on postmortem tissue motor and frontal cortices from 27 patients with ALS and 29 healthy controls were applied to quantify disease-related changes in CNS NA. Sample size was based on availability of tissue samples and transcriptomic data. Patients or families had provided written informed consent.

Statistics

Data are presented as violin plots with all points and expressed as average ± SEM. Mouse data statistical analyses, as well as human LC-MS, were performed on Prism 6 (GraphPad). Multiple *t* tests, one-way or two-way ANOVA, or mixed-effect analyses in the case of missing values, followed by Fischer's least significant difference (LSD) multiple comparisons post hoc tests, were used to compare more than two conditions. Two-sided unpaired Student's *t* tests were used for comparisons between two conditions, two-sided paired Student's *t* tests were used to analyze the PTZ susceptibility and PAC before and after DSP-4 and L-DOPS + benserazide treatments, and one-sided unpaired Student's *t* tests were used for comparisons between two groups of LC-MS human samples. Pearson correlation was used to assess human postmortem NA concentration against the age at death. Human EEG data analyses were performed on JMP Pro 16.0.0 (SAS Institute JMP, Brie Comte Robert, France) using an rmLMM. Multiple regression analyses were performed to test the correlation between MI and patients' clinical features in the same statistical model. Results were considered significant when $P < 0.05$.

Supplementary Materials

This PDF file includes:

Materials and Methods
Figs. S1 to S14
Table S1
References (*79*–*93*)

Other Supplementary Material for this manuscript includes the following:

Data file S1
MDAR Reproducibility Checklist

REFERENCES AND NOTES

1. J. M. Shefner, A. Al-Chalabi, M. R. Baker, L.-Y. Cui, M. de Carvalho, A. Eisen, J. Grosskreutz, O. Hardiman, R. Henderson, J. M. Matamala, H. Mitsumoto, W. Paulus, N. Simon, M. Swash, K. Talbot, M. R. Turner, Y. Ugawa, L. H. van den Berg, R. Verdugo, S. Vucic, R. Kaji, D. Burke, M. C. Kiernan, A proposal for new diagnostic criteria for ALS. *Clin. Neurophysiol.* **131**, 1975–1978 (2020).
2. S. A. Goutman, O. Hardiman, A. Al-Chalabi, A. Chiò, M. G. Savelieff, M. C. Kiernan, E. L. Feldman, Emerging insights into the complex genetics and pathophysiology of amyotrophic lateral sclerosis. *The Lancet Neurology* **21**, 465–479 (2022).
3. N. Geevasinga, P. Menon, P. H. Özdinler, M. C. Kiernan, S. Vucic, Pathophysiological and diagnostic implications of cortical dysfunction in ALS. *Nat. Rev. Neurol.* **12**, 651–661 (2016).
4. S. Vucic, G. A. Nicholson, M. C. Kiernan, Cortical hyperexcitability may precede the onset of familial amyotrophic lateral sclerosis. *Brain : A J. Neurol.* **131**, 1540–1550 (2008).
5. S. Agarwal, G. Koch, A. E. Hillis, W. Huynh, N. S. Ward, S. Vucic, M. C. Kiernan, Interrogating cortical function with transcranial magnetic stimulation: Insights from neurodegenerative disease and stroke. *J. Neurol. Neurosurg. Psychiatry* **90**, 47–57 (2019).
6. A. Brunet, G. Stuart-Lopez, T. Burg, J. Scekic-Zahirovic, C. Rouaux, Cortical circuit dysfunction as a potential driver of amyotrophic lateral sclerosis. *Front. Neurosci.* **14**, (2020).
7. Z. I. Gunes, V. W. Y. Kan, X. Q. Ye, S. Liebscher, Exciting complexity: The role of motor circuit elements in ALS pathophysiology. *Front. Neurosci.* **14**, 1–30 (2020).
8. C. S. Khademullah, A. J. Aqrabawi, K. M. Place, Z. Dargaei, X. Liang, J. C. Pressey, S. Bedard, J. W. Yang, D. Garand, I. Keramidis, A. Gasecka, D. Côté, Y. De Koninck, J. Keith, L. Zinman, J. Robertson, J. C. Kim, M. A. Woodin, Cortical interneuron-mediated inhibition delays the onset of amyotrophic lateral sclerosis. *Brain : A J. Neurol.* **143**, 800–810 (2020).
9. L. A. Reale, M. S. Dyer, S. E. Perry, K. M. Young, T. C. Dickson, A. Woodhouse, C. A. Blizzard, Pathologically mislocalised TDP-43 in upper motor neurons causes a die-forward spread of ALS-like pathogenic changes throughout the mouse corticomotor system. *Prog. Neurobiol.* **226**, 102449 (2023).
10. R. T. Canolty, E. Edwards, S. S. Dalal, M. Soltani, S. S. Nagarajan, H. E. Kirsch, M. S. Berger, N. M. Barbaro, R. T. Knight, High gamma power is phase-locked to theta oscillations in human neocortex. *Science* **313**, 1626–1628 (2006).
11. G. Buzsáki, X.-J. Wang, Mechanisms of gamma oscillations. *Annu. Rev. Neurosci.* **35**, 203–225 (2012).
12. S. Keeley, A. A. Fenton, J. Rinzel, Modeling fast and slow gamma oscillations with interneurons of different subtype. *J. Neurophysiol.* **117**, 950–965 (2017).
13. C. de Hemptinne, E. S. Ryapolova-Webb, E. L. Air, P. A. Garcia, K. J. Miller, J. G. Ojemann, J. L. Ostrem, N. B. Galifianakis, P. A. Starr, Exaggerated phase-amplitude coupling in the primary motor cortex in Parkinson disease. *Proc. Natl. Acad. Sci.* **110**, 4780–4785 (2013).

14. A. Devergnas, M. Caiola, D. Pittard, T. Wichmann, Cortical phase-amplitude coupling in a progressive model of parkinsonism in nonhuman primates. *Cereb. Cortex* **29**, 167–177 (2019).
15. A. Ahnaou, D. Moechars, L. Raeymaekers, R. Biermans, N. V. Manyakov, A. Bottelbergs, C. Wintmolders, K. Kolen, T. Casteele, J. A. Kemp, W. H. Drinkenburg, Emergence of early alterations in network oscillations and functional connectivity in a tau seeding mouse model of Alzheimer's disease pathology. *Sci. Rep.* **7**, (2017).
16. M. S. Goodman, S. Kumar, R. Zomorrodi, Z. Ghazala, A. S. M. Cheam, M. S. Barr, Z. J. Daskalakis, D. M. Blumberger, C. Fischer, A. Flint, L. Mah, N. Herrmann, C. R. Bowie, B. H. Mulsant, T. K. Rajji, Theta-gamma coupling and working memory in Alzheimer's dementia and mild cognitive impairment. *Front. Aging Neurosci.* **10**, 101 (2018).
17. R. Goutagny, N. Gu, C. Cavanagh, J. Jackson, J.-G. Chabot, R. Quirion, S. Krantic, S. Williams, Alterations in hippocampal network oscillations and theta-gamma coupling arise before Aβ overproduction in a mouse model of Alzheimer's disease. *Eur. J. Neurosci.* **37**, 1896–1902 (2013).
18. C. S. Musaeus, Electroencephalographic cross-frequency coupling as a sign of disease progression in patients with mild cognitive impairment: A pilot study. *Front. Neurosci.* **14**, 790 (2020).
19. L. E. Hughes, T. Rittman, T. W. Robbins, J. B. Rowe, Reorganization of cortical oscillatory dynamics underlying disinhibition in frontotemporal dementia. *Brain : A J. Neurol.* **141**, 2486–2499 (2018).
20. J. Scekic-Zahirovic, I. Sanjuan-Ruiz, V. Kan, S. Megat, P. Rossi, S. Dieterlé, R. Cassel, M. Jamet, P. Kessler, D. Wiesner, L. Tzeplaeff, V. Demais, S. Sahadevan, K. M. Hembach, H.-P. Müller, G. Picchiarelli, N. Mishra, S. Antonucci, S. Dirrig-Grosch, J. Kassubek, V. Rasche, A. Ludolph, A.-L. Boutillier, F. Roselli, M. Polymenidou, C. Lagier-Tourenne, S. Liebscher, L. Dupuis, Cytoplasmic FUS triggers early behavioral alterations linked to cortical neuronal hyperactivity and inhibitory synaptic defects. *Nat. Commun.* **12**, 1–19 (2021).
21. K. A. Guttenplan, M. K. Weigel, D. I. Adler, J. Couthouis, S. A. Liddelow, A. D. Gitler, B. A. Barres, Knockout of reactive astrocyte activating factors slows disease progression in an ALS mouse model. *Nat. Commun.* **11**, 1–9 (2020).
22. P. J. Magistretti, I. Allaman, Lactate in the brain: From metabolic end-product to signalling molecule. *Nat. Rev. Neurosci.* **19**, 235–249 (2018).
23. C. Vitrac, M. Benoit-Marand, Monoaminergic modulation of motor cortex function. *Front. Neur. Circ.* **11**, 2195 (2017).
24. C. Dentel, L. Palamiuc, A. Henriques, B. Lannes, O. Spreux-Varoquaux, L. Gutknecht, F. Rene, A. Echaniz-Laguna, J.-L. Gonzalez de Aguilar, K. P. Lesch, V. Meininger, J.-P. Loeffler, L. Dupuis, Degeneration of serotonergic neurons in amyotrophic lateral sclerosis: A link to spasticity. *Brain : A J. Neurol.* **136**, 483–493 (2013).
25. H. El Oussini, J. Scekic-Zahirovic, P. Vercruysse, C. Marques, S. Dirrig-Grosch, S. Dieterlé, G. Picchiarelli, J. Sinniger, C. Rouaux, L. Dupuis, Degeneration of serotonin neurons triggers spasticity in amyotrophic lateral sclerosis. *Ann. Neurol.* **82**, 444–456 (2017).
26. J. Lotharius, P. Brundin, Pathogenesis of Parkinson's disease: Dopamine, vesicles and α-synuclein. *Nat. Rev. Neurosci.* **3**, 932–942 (2002).
27. N. Holland, T. W. Robbins, J. B. Rowe, The role of noradrenaline in cognition and cognitive disorders. *Brain : A J. Neurol.* **144**, 2243–2256 (2021).
28. A. C. Peterson, C.-S. R. Li, Noradrenergic dysfunction in Alzheimer's and Parkinson's diseases—An overview of imaging studies. *Front. Aging Neurosci.* **10**, 127 (2018).
29. M. E. Ripps, G. W. Huntley, P. R. Hof, J. H. Morrison, J. W. Gordon, Transgenic mice expressing an altered murine superoxide dismutase gene provide an animal model of amyotrophic lateral sclerosis. *Proc. Natl. Acad. Sci. U.S.A.* **92**, 689–693 (1995).
30. J. Scekic-Zahirovic, H. El Oussini, S. Mersmann, K. Drenner, M. Wagner, Y. Sun, K. Allmeroth, S. Dieterlé, J. Sinniger, S. Dirrig-Grosch, F. Rene, D. Dormann, C. Haass, A. C. Ludolph, C. Lagier-Tourenne, E. Storkebaum, L. Dupuis, Motor neuron intrinsic and extrinsic mechanisms contribute to the pathogenesis of FUS-associated amyotrophic lateral sclerosis. *Acta Neuropathol.* **133**, 887–906 (2017).
31. C. Marques, T. Burg, J. Scekic-Zahirovic, M. Fischer, C. Rouaux, Upper and lower motor neuron degenerations are somatotopically related and temporally ordered in the Sod1 mouse model of amyotrophic lateral sclerosis. *Brain Sci.* **11**, 1–18 (2021).
32. J. Van Erum, D. Van Dam, P. P. De Deyn, PTZ-induced seizures in mice require a revised Racine scale. *Epilepsy Behav.* **95**, 51–55 (2019).
33. S. Maeda, B. Djukic, P. Taneja, G.-Q. Yu, I. Lo, A. Davis, R. Craft, W. Guo, X. Wang, D. Kim, R. Ponnusamy, T. M. Gill, E. Masliah, L. Mucke, Expression of A152T human tau causes age- dependent neuronal dysfunction and loss in transgenic mice. *EMBO Rep.* **17**, 530–551 (2016).
34. N. A. Copping, A. Adhikari, S. P. Petkova, J. L. Silverman, Genetic backgrounds have unique seizure response profiles and behavioral outcomes following convulsant administration. *Epilepsy Behav.* **101**, 106547 (2019).
35. R. A. Kohnken, D. J. Schwahn, Lack of chronic histologic lesions supportive of sublethal spontaneous seizures in FVB/N mice. *Comp. Med.* **66**, 105–111 (2016).
36. H. M. Chameh, S. Rich, L. Wang, F.-D. Chen, L. Zhang, P. L. Carlen, S. J. Tripathy, T. A. Valiante, Diversity amongst human cortical pyramidal neurons revealed via their sag currents and frequency preferences. *Nat. Commun.* **12**, 1–15 (2021).
37. C. M. Florez, R. J. McGinn, V. Lukankin, I. Marwa, S. Sugumar, J. Dian, L. N. Hazrati, P. L. Carlen, L. Zhang, T. A. Valiante, In vitro recordings of human neocortical oscillations. *Cereb. Cortex* **25**, 578–597 (2015).
38. N. W. Johnson, M. Özkan, A. P. Burgess, E. J. Prokic, K. A. Wafford, M. J. O'Neill, S. D. Greenhill, I. M. Stanford, G. L. Woodhall, Phase-amplitude coupled persistent theta and gamma oscillations in rat primary motor cortex in vitro. *Neuropharmacology* **119**, 141–156 (2017).
39. N. Rustamov, J. Humphries, A. Carter, E. C. Leuthardt, Theta-gamma coupling as a cortical biomarker of brain-computer interface-mediated motor recovery in chronic stroke. *Brain Commun* **4**, 1–18 (2022).
40. R. K. Spooner, T. W. Wilson, Cortical theta–gamma coupling governs the adaptive control of motor commands. *Brain Commun* **4**, 1–12 (2022).
41. A. B. L. Tort, R. Komorowski, H. Eichenbaum, N. Kopell, Measuring phase-amplitude coupling between neuronal oscillations of different frequencies. *J. Neurophysiol.* **104**, 1195–1210 (2010).
42. A. B. L. Tort, M. A. Kramer, C. Thorn, D. J. Gibson, Y. Kubota, A. M. Graybiel, N. J. Kopell, Dynamic cross-frequency couplings of local field potential oscillations in rat striatum and hippocampus during performance of a T-maze task. *Proc. Natl. Acad. Sci.* **105**, 20517–20522 (2008).
43. C. Scheffzük, V. I. Kukushka, A. L. Vyssotski, A. Draguhn, A. B. L. Tort, J. Brankačk, Selective coupling between theta phase and neocortical fast gamma oscillations during REM-sleep in mice. *PLOS ONE* **6**, e28489 (2011).
44. J. A. Hoskins, L. J. Davis, The acute effect on levels of catecholamines and metabolites in brain, of a single dose of MPTP in 8 strains of mice. *Neuropharmacology* **28**, 1389–1397 (1989).
45. P.-O. Polack, J. Friedman, P. Golshani, Cellular mechanisms of brain state-dependent gain modulation in visual cortex. *Nat. Neurosci.* **16**, 1331–1339 (2013).
46. J. Reimer, M. J. McGinley, Y. Liu, C. Rodenkirch, Q. Wang, D. A. McCormick, A. S. Tolias, Pupil fluctuations track rapid changes in adrenergic and cholinergic activity in *cortex. Communications* **7**, 1–7 (2016).
47. J. M. Fritschy, R. Grzanna, Selective effects of DSP-4 on locus coeruleus axons: Are there pharmacologically different types of noradrenergic axons in the central nervous system? *Prog. Brain Res.* **88**, 257–268 (1991).
48. S. A. Thomas, B. T. Marck, R. D. Palmiter, A. M. Matsumoto, Restoration of norepinephrine and reversal of phenotypes in mice lacking dopamine fi-hydroxylase. *J. Neurochem.* **70**, 20468–20476 (1998).
49. N. R. Jabir, C. K. Firoz, T. A. Zughaibi, M. A. Alsaadi, A. M. Abuzenadah, A. I. Al-Asmari, A. Alsaieedi, B. A. Ahmed, A. K. Ramu, S. Tabrez, A literature perspective on the pharmacological applications of yohimbine. *Ann. Med.* **54**, 2849–2863 (2023).
50. D. Zhang, S. Chen, S. Xu, J. Wu, Y. Zhuang, W. Cao, X. Chen, X. Li, The clinical correlation between Alzheimer's disease and epilepsy. *Front. Neurol.* **13**, 922535 (2022).
51. D. Schijven, R. Stevelink, M. McCormack, W. van Rheenen, J. J. Luykx, B. P. C. Koeleman, J. H. Veldink; Project MinE ALS GWAS Consortium; International League Against Epilepsy Consortium on Complex Epilepsies, Analysis of shared common genetic risk between amyotrophic lateral sclerosis and epilepsy. *Neurobiol. Aging* **92**, 153.e1–153.e5 (2020).
52. A. M. García-Cabrero, R. Guerrero-López, B. G. Giráldez, M. Llorens-Martín, J. Ávila, J. M. Serratosa, M. P. Sánchez, Hyperexcitability and epileptic seizures in a model of frontotemporal dementia. *Neurobiol. Dis.* **58**, 200–208 (2013).
53. V. Gomez-Murcia, U. Sandau, B. Ferry, S. Parrot, C. Laurent, M. Basquin, L. Buée, D. Boison, D. Blum, Hyperexcitability and seizures in the THY-Tau22 mouse model of tauopathy. *Neurobiol. Aging* **94**, 265–270 (2020).
54. Y. Salimpour, Cross-frequency coupling based neuromodulation for treating neurological disorders. *Front. Neurosci.* **13**, 125 (2019).
55. A. Malekshahi, U. Chaudhary, A. Jaramillo-Gonzalez, A. Lucas Luna, A. Rana, A. Tonin, N. Birbaumer, S. Gais, Sleep in the completely locked-in state (CLIS) in amyotrophic lateral sclerosis. *Sleep* **42**, (2019).
56. A. Secco, A. Tonin, A. Rana, A. Jaramillo-Gonzalez, M. Khalili-Ardali, N. Birbaumer, U. Chaudhary, EEG power spectral density in locked-in and completely locked-in state patients: A longitudinal study. *Cognit. Neurodyn.* **15**, 473–480 (2020).
57. Q. Gu, Neuromodulatory transmitter systems in the cortex and their role in cortical plasticity. *Neuroscience* **111**, 815–835 (2002).
58. E. Sofic, P. Riederer, W. Gsell, M. Gavranovic, A. Schmidtke, K. Jellinger, Biogenic amines and metabolites in spinal cord of patients with Parkinson's disease and amyotrophic lateral sclerosis. *J. Neural Transm.* **3**, 133–142 (1991).
59. O. Bertel, S. Malessa, E. Sluga, O. Hornykiewicz, Amyotrophic lateral sclerosis: Changes of noradrenergic and serotonergic transmitter systems in the spinal cord. *Brain Res.* **566**, 54–60 (1991).
60. B. R. Brooks, M. G. Ziegler, C. R. Lake, J. H. Wood, S. J. Enna, W. K. Engel, Cerebrospinal fluid norepinephrine and free γ-aminobutyric acid in amyotrophic lateral sclerosis. *Brain Res. Bull.* **5**, 765–768 (1980).
61. M. G. Ziegler, B. R. Brooks, C. R. Lake, J. H. Wood, S. J. Enna, Norepinephrine and gamma-aminobutyric acid in amyotrophic lateral sclerosis. *Neurology* **30**, 98–101 (1980).

62. V. P. Barkhatova, I. A. Zavalishin, A. V. Kostiuk, E. G. Demina, T. A. Moskvitina, Neurotransmitter changes in amyotrophic lateral sclerosis. *Zh. Nevrol. Psikhiatr. Im. S S Korsakova* **96**, 78–85 (1996).
63. W. Hoogendijk, C. W. Pool, D. Troost, E. van Zwieten, Image analyser-assisted morphometry of the locus coeruleus in Alzheimer's disease, Parkinson's disease and amyotrophic lateral sclerosis. *Brain : A J. Neurol.* **118**, 131–143 (1995).
64. R. W. Orrell, A. W. King, D. A. Hilton, M. J. Campbell, R. J. Lane, J. S. de Belleroche, Familial amyotrophic lateral sclerosis with a point mutation of SOD-1: Intrafamilial heterogeneity of disease duration associated with neurofibrillary tangles. *J. Neurol. Neurosurg. Psychiatry* **59**, 266–270 (1995).
65. J. Brettschneider, K. Del Tredici, J. B. Toledo, J. L. Robinson, D. J. Irwin, M. Grossman, E. Suh, V. M. Van Deerlin, E. M. Wood, Y. Baek, L. Kwong, E. B. Lee, L. Elman, L. McCluskey, L. Fang, S. Feldengut, A. C. Ludolph, V. M. Y. Lee, H. Braak, J. Q. Trojanowski, Stages of pTDP-43 pathology in amyotrophic lateral sclerosis. *Ann. Neurol.* **74**, 20–38 (2013).
66. M. Van Egroo, E. Koshmanova, G. Vandewalle, H. I. L. Jacobs, Importance of the locus coeruleus-norepinephrine system in sleep-wake regulation: Implications for aging and Alzheimer's disease. *Sleep Med. Rev.* **62**, 101592 (2022).
67. H. Salgado, M. Treviño, M. Atzori, Layer- and area-specific actions of norepinephrine on cortical synaptic transmission. *Brain Res.* **1641**, 163–176 (2016).
68. B. Feinstein, C. A. Gleason, B. Libet, Stimulation of locus coeruleus in man Preliminary trials for spasticity and epilepsy. *Stereotact Funct. Neurosurg.* **52**, 26–41 (1989).
69. G. K. Weiss, J. Lewis, C. Jimenez-Rivera, A. Vigil, M. E. Corcoran, Antikindling effects of locus coeruleus stimulation: Mediation by ascending noradrenergic projections. *Exp. Neurol.* **108**, 136–140 (1990).
70. G. Ferraro, P. Sardo, M. Sabatino, G. Caravaglios, V. La Grutta, Anticonvulsant activity of the noradrenergic locus coeruleus system: Role of beta mediation. *Neurosci. Lett.* **169**, 93–96 (1994).
71. P. K. Mishra, R. L. Burger, A. F. Bettendorf, R. A. Browning, P. C. Jobe, Role of norepinephrine in forebrain and brainstem seizures: Chemical lesioning of locus ceruleus with DSP4. *Exp. Neurol.* **125**, 58–64 (1994).
72. P. Szot, D. Weinshenker, S. S. White, C. A. Robbins, N. C. Rust, P. A. Schwartzkroin, R. D. Palmiter, Norepinephrine-deficient mice have increased susceptibility to seizure-inducing stimuli. *J. Neurosci.* **19**, 10985–10992 (1999).
73. V. A. Nazarova, A. V. Sokolov, V. N. Chubarev, V. V. Tarasov, H. B. Schiöth, Treatment of ADHD: Drugs, psychological therapies, devices, complementary and alternative methods as well as the trends in clinical trials. *Front. Pharmacol.* **13**, 1066988 (2022).
74. A. Montoya, R. Bruins, M. A. Katzman, P. Blier, The noradrenergic paradox: Implications in the management of depression and anxiety. *Neuropsychiatr. Dis. Treat.* **12**, 541–557 (2016).
75. M. E. Heidari, J. Nadali, A. Parouhan, M. Azarafraz, S. M. Tabatabai, S. S. N. Irvani, F. Eskandari, A. Gharebaghi, Prevalence of depression among amyotrophic lateral sclerosis (ALS) patients: A systematic review and meta-analysis. *J. Affect. Disord.* **287**, 182–190 (2021).
76. J. M. Statland, D. Moore, Y. Wang, M. Walsh, T. Mozaffar, L. Elman, S. P. Nations, H. Mitsumoto, J. A. Fernandes, D. Saperstein, G. Hayat, L. Herbelin, C. Karam, J. Katz, H. M. Wilkins, A. Agbas, R. H. Swerdlow, R. M. Santella, M. M. Dimachkie, R. J. Barohn, Rasagiline Investigators of the Muscle Study Group and Western ALS Consortium, Rasagiline for amyotrophic lateral sclerosis: A randomized, controlled trial. *Muscle Nerve* **59**, 201–207 (2019).
77. E. Dalla Bella, E. Bersano, G. Antonini, G. Borghero, M. Capasso, C. Caponnetto, A. Chiò, M. Corbo, M. Filosto, F. Giannini, R. Spataro, C. Lunetta, J. Mandrioli, S. Messina, M. R. Monsurrò, G. Mora, N. Riva, R. Rizzi, G. Siciliano, V. Silani, I. Simone, G. Sorarù, V. Tugnoli, L. Verriello, P. Volanti, R. Furlan, J. M. Nolan, E. Abgueguen, I. Tramacere, G. Lauria, The unfolded protein response in amyotrophic later sclerosis: Results of a phase 2 trial. *Brain : A J. Neurol.* **144**, 2635–2647 (2021).
78. X. Li, D. D. Koeberl, M. W. Lutz, R. Bedlack, Clenbuterol treatment is safe and associated with slowed disease progression in a small open-label trial in patients with amyotrophic lateral sclerosis. *J. Clin. Neuromuscul. Dis.* **24**, 214–221 (2023).
79. K. Kam, Á. M. Duffy, J. Moretto, J. J. LaFrancois, H. E. Scharfman, Interictal spikes during sleep are an early defect in the Tg2576 mouse model of β-amyloid neuropathology. *Sci. Rep.* **6**, 1 (2016).
80. H. Bokil, P. Andrews, J. E. Kulkarni, S. Mehta, P. P. Mitra, Chronux: A platform for analyzing neural signals. *J. Neurosci. Methods* **192**, 146–151 (2010).
81. B. R. Brooks, R. G. Miller, M. Swash, T. L. Munsat, World Federation of Neurology Research Group on Motor Neuron Diseases, in (2000), vol. 1, pp. 293–299.
82. S. Sangari, I. Peyre, A. Lackmy-Vallée, E. Bayen, P.-F. Pradat, V. Marchand-Pauvert, Transient increase in recurrent inhibition in amyotrophic lateral sclerosis as a putative protection from neurodegeneration. *Acta Physiol* **234**, e13758 (2022).
83. A. Delorme, S. Makeig, EEGLAB: An open source toolbox for analysis of single-trial EEG dynamics including independent component analysis. *J. Neurosci. Methods* **134**, 9–21 (2004).
84. O. Bertrand, F. Perrin, J. Pernier, A theoretical justification of the average reference in topographic evoked potential studies. *Electroencephalogr. Clin. Neurophysiol.* **62**, 462–464 (1985).
85. A. Delorme, T. Sejnowski, S. Makeig, Enhanced detection of artifacts in EEG data using higher-order statistics and independent component analysis. *Neuroimage* **34**, 1443–1449 (2007).
86. S. Makeig, A. J. Bell, T.-P. Jung, T. J. Sejnowski, Complex independent component analysis of frequency-domain electroencephalographic data. *NIPS* **16**, 1311–1323 (1995).
87. R. Martínez-Cancino, J. Heng, A. Delorme, K. Kreutz-Delgado, R. C. Sotero, S. Makeig, Measuring transient phase-amplitude coupling using local mutual information. *Neuroimage* **185**, 361–378 (2019).
88. M. Kremer, I. Yalcin, Y. Goumon, X. Wurtz, L. Nexon, D. Daniel, S. Megat, R. A. Ceredig, C. Ernst, G. Turecki, V. Chavant, J.-F. Théroux, A. Lacaud, L.-E. Joganah, V. Lelievre, D. Massotte, P.-E. Lutz, R. Gilsbach, E. Salvat, M. Barrot, A dual noradrenergic mechanism for the relief of neuropathic allodynia by the antidepressant drugs duloxetine and amitriptyline. *J. Neurosci.* **38**, 9934–9954 (2018).
89. D. L. Lin, W. T. Chang, T. L. Kuo, R. H. Liu, Chemical derivatization and the selection of deuterated internal standard for quantitative determination—Methamphetamine example*. *J. Anal. Toxicol.* **24**, 275–280 (2000).
90. S. Liebscher, G. B. Keller, P. M. Goltstein, T. Bonhoeffer, M. Hübener, Selective persistence of sensorimotor mismatch signals in visual cortex of behaving Alzheimer's disease mice. *Curr. Biol.* **26**, 956–964 (2016).
91. A. Dobin, C. A. Davis, F. Schlesinger, J. Drenkow, C. Zaleski, S. Jha, P. Batut, M. Chaisson, T. R. Gingeras, STAR: Ultrafast universal RNA-seq aligner. *Bioinformatics* **29**, 15–21 (2013).
92. S. Orjuela, R. Huang, K. M. Hembach, M. D. Robinson, C. Soneson, ARMOR: An Automated Reproducible MOdular workflow for preprocessing and differential analysis of RNA-seq data. *G3 (Bethesda)* **9**, 2089–2096 (2019).
93. C. Rouaux, I. Panteleeva, F. Rene, J.-L. Gonzalez de Aguilar, A. Echaniz-Laguna, L. Dupuis, Y. Menger, A.-L. Boutillier, J.-P. Loeffler, Sodium valproate exerts neuroprotective effects in vivo through CREB-binding protein-dependent mechanisms but does not improve survival in an amyotrophic lateral sclerosis mouse model. *J. Neurosci.* **27**, 5535–5545 (2007).

Acknowledgments: We are extremely grateful to all patients with ALS and healthy volunteers who participated in the study. We are thankful to A. Picchinenna and C. de Tapia for technical assistance (Inserm U1329, Université de Strasbourg), A. Lackmy-Vallée (LIB, Sorbonne Université) and C. Gitton (CENIR-EEG/MEG platform, Brain Institute ICM, Paris) for technical assistance to collect rsEEG, M. Chaumon (CENIR-EEG/MEG platform, Brain Institute ICM, Paris) for valuable help for EEG preprocessing, and A. Giron (LIB, Sorbonne Université) for valuable advice for rsEEG statistical analysis. We thank the Hôpital de la Pitié-Salpêtrière and Brainbank Neuro-CEB Neuropathology Network [F. Letournel (CHU Angers), M.-L. Martin-Négrier (CHU Bordeaux), F. Chapon (CHU Caen), C. Godfraind (CHU Clermont-Ferrand), C.-A. Maurage (CHU Lille), V. Deramecourt (CHU Lille), D. Meyronnet (CHU Lyon), N. Streichenberger (CHU Lyon), A. M. de Paula (CHU Marseille), V. Rigau (CHU Montpellier), F. Vandenbos-Burel (Nice), C. Duyckaerts (CHU PS Paris), D. Seilhean (CHU PS, Paris), S. Boluda (CHU PS, Paris), I. Plu (CHU PS, Paris), S. Milin (CHU Poitiers), D. Christian Chiforeanu (CHU Rennes), A. Laquerrière (CHU Rouen), and B. Lannes (CHU Strasbourg)] for providing human tissues. **Funding:** The work has been supported by a European Research Council starting grant #639737 (C.R.), Association pour la Recherche sur la Sclérose Latérale Amyotrophique (C.R. and R.G.), Agence Nationale de la Recherche- Deutsche Forschungsgemeinschaft ANR-21-CE37-0033-01 (C.R., S.L., V.M.-P., and R.G.), post-doctoral fellowship from the Association Française contre les Myopathies-Téléthon #21993 (J.S.-Z.), PhD fellowships from the French Ministry of Scientific Research and Innovation (C.B. and A.B.), 4th year PhD fellowship from the Association pour la Recherche sur la Sclérose Latérale Amyotrophique (ARSLA) (C.B.), Cluster for Systems Neurology-EXC 2145 SyNergy- ID 390857198 (S.L.), the Emmy Noether Program of the German Research Foundation (S.L.), and Deutsche Gesellschaft für Muskelkranke e.V. (S.L.). The Brainbank Neuro-CEB Neuropathology Network is supported by the following associations: ARSLA, CSC, France DFT, Fondation ARSEP, Fondation Vaincre Alzheimer, France Parkinson, and German Research Foundation under Germany's Excellence Strategy within the framework of the Munich. **Author contributions:** C.R., S.L., and V.M.-P. conceptualized the study, with intellectual contributions from L.D. and F.R. J.S.-Z. and G.S.-L. performed ECoG recordings and analyzed the data together with V.D., J.G., S.J.G., J.S., and M.F. and the expertise of R.G. P.-F.P. enrolled patients with ALS and controls and performed the clinical evaluation. V.M.-P. and C.B. performed EEG recordings and analyzed the data. A.B. and V.A. performed LC-MS measurements with the expertise of Y.G. A.B., S.D.-G., C.G., M.T., and S.D. performed qPCR, Western blot, and immunofluorescence experiments, and A.B., S.D.-G., and S.D. analyzed the data with image analyses tools designed by P.K. G.S.-L. and C.G. treated the animals and performed the survival analyses. Z.G. processed human tissue samples. S.M. performed transcriptomic analysis on human data. E.L., V.W.Y.K., and X.Y. performed in vivo two-photon imaging; X.Y. and S.L. analyzed and visualized in vivo two-photon imaging data. C.R., S.L., and V.M.-P. supervised the study and secured funding. C.R. and S.L. prepared the figures. The manuscript was drafted by C.R., S.L., and V.M.-P. and reviewed and accepted by all authors. **Competing interests:** The authors declare that they have no competing interests. **Data and materials availability:** All data associated with this

study are present in the paper or the Supplementary Materials. The patient raw datasets cannot be made publicly available because of the data protection concerns regarding potentially identifying and sensitive patient information, but EEG raw data from the clinical study can be made available to qualified researchers from V.M.-P. and P.-F.P., in agreement with Inserm and the French National Committee for the Protection of Individuals.

Submitted 19 December 2022
Resubmitted 7 November 2023
Accepted 20 February 2024
Published 13 March 2024
10.1126/scitranslmed.adg3665